lubricants

MDPI

Article

Thermal Tribo-Dynamic Behaviors of Water-Lubricated Bearings during Start-Up with Journal Shape Error

Shouan Chen, Jianlin Cai *, Junfu Zhang and Zaixin Liu

College of Mechanical Engineering, Xihua University, Chengdu 610039, China; 0120230099@mail.xhu.edu.cn (S.C.); zhangjf@mail.xhu.edu.cn (J.Z.); 0120040023@mail.xhu.edu.cn (Z.L.)
* Correspondence: jl_cai@mail.xhu.edu.cn

Abstract: In practical scenarios, journal bearings often exhibit shape errors due to machining imperfections and operational wear. These deviations from perfect roundness can significantly impact the performance of journal bearings during start-up. This study investigates the impact of journal shape errors on transient mixed lubrications, such as water film temperature and asperity contact, as well as on the rotor dynamics of water-lubricated bearings (WLB) at start-up. The simulation results of the developed numerical model are compared with the experimental data from existing studies to verify their accuracy. Following this validation, parametric analyses are conducted using the model. The analytical results indicate that journal shape error increases the temperature rise of the water-lubricated bearing system during start-up. The greater the error in journal shape, the higher the temperature rise, both in terms of shape amplitude and waviness order. Interestingly, the thermal deformation caused by the temperature effect decreases the vertical displacement during start-up. The study also finds that higher start-up speeds lead to quicker temperature increases when shape errors are present. However, these speeds enable the bearing to more rapidly reach the elastohydrodynamic lubrication (EHL) stage, where the temperature rise stabilizes. Therefore, start-up speeds must be carefully selected.

Keywords: thermal characteristic; tribo-dynamic behavior; start-up; journal shape error

Citation: Chen, S.; Cai, J.; Zhang, J.; Liu, Z. Thermal Tribo-Dynamic Behaviors of Water-Lubricated Bearings during Start-Up with Journal Shape Error. *Lubricants* **2024**, *12*, 106. https://doi.org/10.3390/lubricants12040106

Received: 15 February 2024
Revised: 16 March 2024
Accepted: 21 March 2024
Published: 23 March 2024

1. Introduction

WLB systems have a broad range of applications in underwater vehicles, and their performance significantly impacts the vehicle's stability and safety [1,2]. Thus, the performance of water-lubricated bearings is easily affected by changes in parameters like radius clearance, thickness of the water film, operating temperature, and surface roughness [3]. Most scholars in the WLB research often focus on the theoretical design of water lubrication bearings, processing and manufacturing, assembly, and other aspects, and usually regard the journal as an ideal round [4]. However, in practical engineering, processing errors, wear, and other factors often affect the surface shape of the rotor shaft, leading to inherent errors in the micron-level journal waviness and presenting as a non-ideal circular shape. Due to the mixed lubrication condition of WLBs, the amplitude of the journal shape error is on the order of microns with respect to the radius clearance and the minimum water film thickness; it is also one of the crucial factors impacting the tribo-dynamic behaviors of WLBs. Particularly during WLB start-up, journal shape error will exacerbate friction and adhesive wear at the contact interface, increasing the operating temperature and deteriorating the service life of the bearing [5]. Therefore, when temperature variations are involved, it is crucial to examine the impact of journal shape error on the transient lubrication performance and dynamic response in the start-up state of the WLB system to enhance bearing performance and lifespan.

During the start-up state, a complex correlation exists between the bearing rotor's dynamic characteristics and the contacting surface's transient mixed elastohydrodynamic

lubrication properties. A plethora of scholarly research has been conducted, both experimentally and theoretically, to explore this connection in depth [3,5–16]. Mokhtar et al. [5,6] experimentally measured and observed the axial trajectory and wear during the start-up state of a fluid dynamic pressure bearing, and the observed results showed that the sliding wear phenomenon primarily occurs at start-up state and is mitigated after reaching the EHL state. Fillon's research team analyzed the tribological characteristics of journal bearings during the start-up state by developing a mathematical model for thermoelastohydrodynamic lubrication (TEHL) of radial dynamic bearings and then conducted the corresponding tests [7,8]. However, Fillon's theoretical study did not consider the roughness factor of the contact surfaces of the rotor shaft and the bushing, so the analytical results obtained may have some errors [9]. To address this problem, Cui et al. [10,11] used the average Reynolds equation [12] and Greenwood–Williamson model [13] to introduce the surface roughness factor and combined the lubrication model with the rotor dynamics equation to construct a transient mixed elastohydrodynamic lubrication model. Through simulation analysis of Cui et al.'s theoretical model [10,11], it was discovered that the contact force and contact time decreased as the relative clearance of the journal bearing increased. However, in his study, Cui did not account for the transient thermal behavior during the start-up state of the bearing. Inspired by the above studies, Xiang and Han [14] developed a transient which combines the lubrication equation and the rotor dynamics equation to analyze the mixed thermoelastohydrodynamic lubrication behavior of journal bearings and revealed that neglecting thermal characteristics may lead to underestimating the dynamic contact load during startup. Subsequently, Xiang et al. [15,16] studied the frictional dynamics of WLBs with unbalanced rotors. Thus, it can be inferred that journal shape errors (of the same order of amplitude as the rotor imbalance) substantially affect the mixed friction behavior of WLBs. However, a limited number of studies have focused on the impact of journal shape error on the lubrication performance and dynamic behavior of WLBs during the start-up state.

Most scholarly studies on journal shape errors have primarily focused on types such as aerostatic bearings [17–19], hydrostatic bearings [20], and hybrid journal bearings [21]. The parameters studied in the literature include journal roughness [22], journal waviness [23–25], journal roundness error [26], journal misalignment (wear, texture, profile modifications) [27–29], etc. Among them, Minseok et al. [17] investigated the dynamic behavior and time–frequency properties of gas cylindrical journal bearings in the presence of shape errors in both journals and bearings. The research findings indicate that precision of journal manufacturing holds greater significance than the precision of bearing manufacturing. Peng's research team [23,24] investigated the effect of three-dimensional surface waviness of bush on the static–dynamic properties of aerostatic plain bearings. However, the studies mentioned above were conducted from a tribological perspective and did not account for the dynamic behavior of the journal rotor. Hence, Cai et al. [25] combined journal shape error and bearing wear to investigate their effects on the tribo-dynamic behavior of WLBs and found that the effect of journal shape error on the tribo-dynamics behavior is more remarkable than that of bearing wear. At the same time, Sun et al. [30] conducted experimental research exploring the effects of shaft shape errors on the journal dynamics behavior of the bearing system. Recently, Chen and Xiang [31] investigated the evolution on the transient tribo-dynamic behavior of bearings with the variation in journal shape error by developing a tribo-dynamic model of WLBs during the start-up state. However, the thermal effects of the mixed friction behavior were not considered in their model, and therefore, the results obtained by the study may be less precise [14,31]. Hence, the tribo-dynamic responses of WLBs with journal shape errors must be studied in depth, considering thermal characteristics during start-up.

In this paper, a tribo-dynamics model of WLBs is established to investigate the effect of journal shape error on the start-up performance by considering the coupling characteristics of fluid–solid–thermal interactions, which has not been reported in any research. The numerical analysis results of the proposed model show that the journal shape error

exacerbates the temperature increase during start-up. However, thermal deformation reduces the lubrication gap and increases the hydrodynamic effect, thus improving the lubrication performance. Meanwhile, the higher the bearing start-up speed, the faster the rise in temperature and the larger the shaft trajectory. Conversely, lower speeds result in higher contact forces. Therefore, start-up speeds need to be carefully selected. The above study results will serve as a reliable reference for bearing design.

2. Mathematic Model

2.1. Transient Lubrication Gap

The object of this paper is a water-lubricated radial bearing with PEEK as the material of the bush, whose geometry and analyzed coordinate system during the start-up state are shown in Figure 1. In Figure 1, O_J and O_B are the geometric center of the WLB and the transient center position of the journal, respectively. e is expressed as the eccentric distance between the geometric center and transient center position. During startup, the transient lubrication gap at the contact interface is a superposition of nonlinear quantities such as transient elastic deformation, thermal deformation, and rotor trajectory. The governing equation is described as [31]:

$$h(\theta,z,t) = C(1+\varepsilon(t)\cos(\theta(t)-\varphi(t))) + \delta_{BE}(\theta,z,t,p) + \Delta_{SE}(\theta,t) \\ +\delta_{BT}(\theta,z,t,\Delta T,p) + \delta_{JT}(\theta,z,t,\Delta T,p) \quad (1)$$

where C and Δ_{SE} are the radius clearance between journal and bearing and journal shape error, respectively; $\varphi(t)$ and $\varepsilon(t)$ are the time-varying attitude angle and eccentricity, respectively; δ_{BE} is the bush elastic deformation; and δ_{BT} and δ_{JT} are the deformations of the bush and journal caused by thermal effects, respectively.

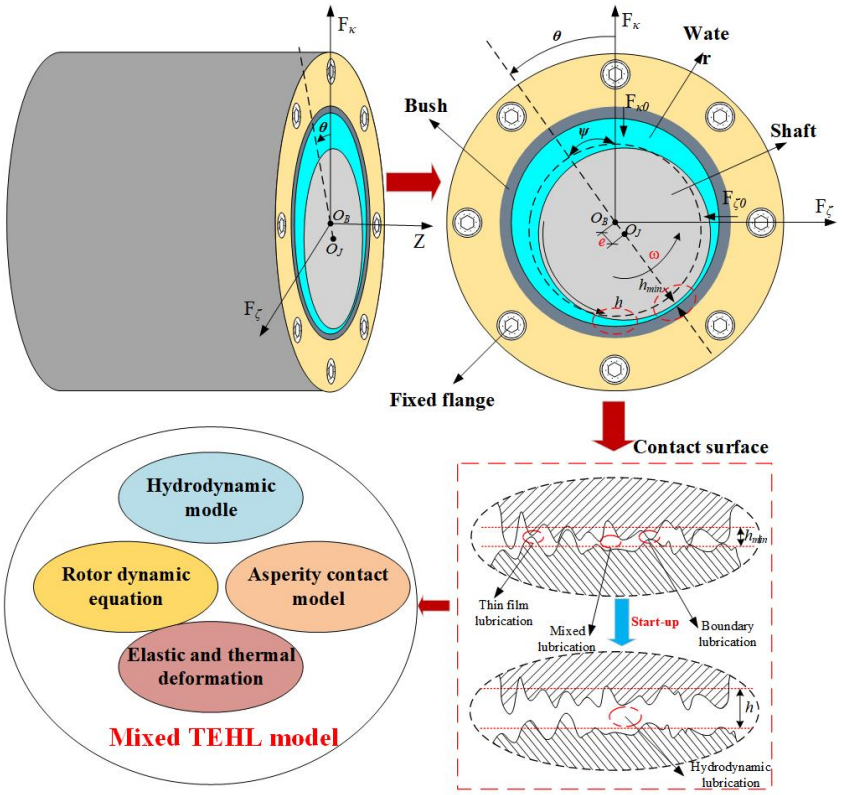

Figure 1. Geometry of water-lubricated bearings system.

According to the literature on the study of journal shape errors [25,30,31], the shaft system is primarily processed using the turning method, resulting in a wavy and undulating surface shape due to machining errors, wear, and deformations in operation, while the

surface roughness peaks appear randomly. In this way, a sinusoidal function with a period of $2\pi/n$ is used to simulate the error in the journal shape [32]. Thus, the time-varying sinusoidal function is expressed as

$$\sin(\theta, t) = (r_1 - r_2)\sin(n\theta - n\omega t) \tag{2}$$

where ω and n are the rotation speed and the waviness order of the journal shape, respectively. As displayed in Figure 2, the actual and ideal circular journal surface profile are represented by r_1 and r_2, respectively. Eventually, $\delta_{SE}(\theta, t)$ is presented by

$$\Delta_{SE}(\theta, t) = C\Delta r[1 + 0.5\sin(n\theta - n\omega t)] \tag{3}$$

where $\Delta r = \delta r/C$ represent the dimensionless amplitude of the journal shape error relative to the radius clearance. As shown in Figure 2, at n = 0, the journal surface profile can be considered as an ideal circle.

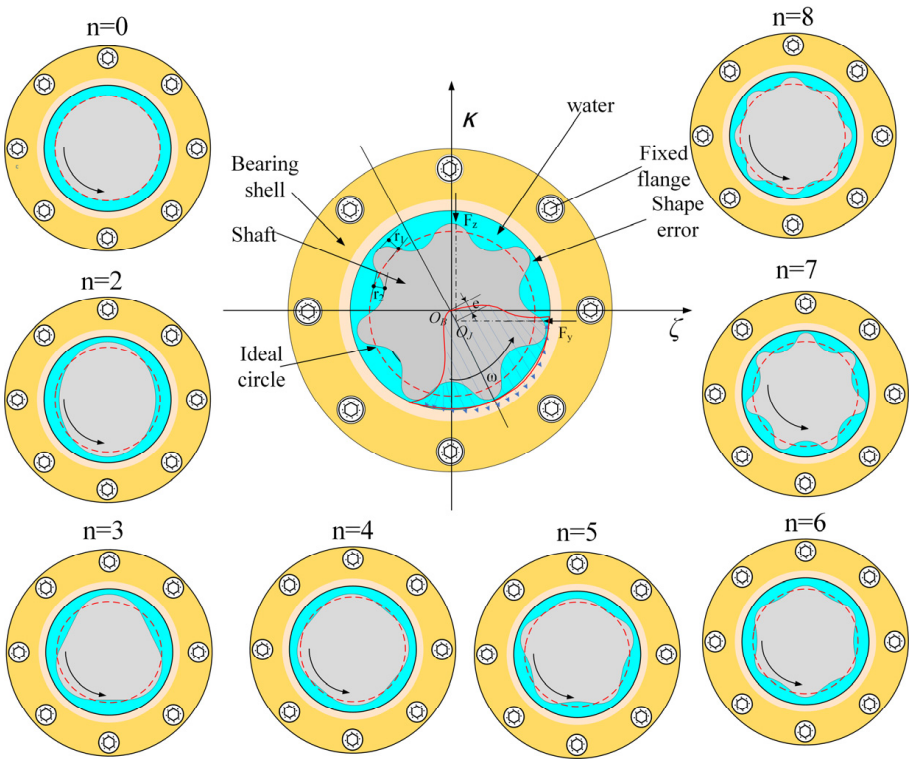

Figure 2. Schematic diagram of water-lubricated bearing system with journal shape error.

2.2. Dynamic Equations

The transient journal trajectory during the start-up state of the WLB is determined by a series of rotor dynamics equations considering both hydrodynamic and contact forces. Based on the bearing coordinate system shown in Figure 1 and Newton's law, the transient dynamic behavior of the journal is governed by the subsequent equations, while assuming a rigid journal.

$$\begin{cases} m_J\kappa'' = W + F_{fric\kappa}(t) - F_{h\kappa}(t) - F_{c\kappa}(t) - \mathrm{m}_J\omega^2 r\cos\left(\frac{\pi\omega t}{30}\right) \\ m_J\zeta'' = F_{h\zeta}(t) + F_{c\zeta}(t) + F_{fric\zeta}(t) + \mathrm{m}_J\omega^2 r\sin\left(\frac{\pi\omega t}{30}\right) \end{cases} \tag{4}$$

where m_J and W are the rotor mass and static load, respectively; F represents the dynamic forces (including transient hydrodynamic pressure force, contact force, and mixed friction force); the subscripts κ and ζ indicate the direction of the coordinate system; the subscripts h and c denote hydrodynamic and contact, respectively; the subscript *fric* represents friction; and t and r are the start-up time and rotor unbalance.

The calculation methods of hydrodynamic F_h and contact force F_c described in Equation (4) are given in detail in Sections 2.3 and 2.5.

2.3. Transient Hydrodynamic Model

2.3.1. Transient Reynolds Equation

During bearing start-up, asperity of the contact surfaces can disrupt the fluid flow between bush and journal, potentially affecting the lubrication performance. Thus, the average Reynolds equation [12] was employed as the lubrication control equation to evaluate the effect of roughness on fluid by the ratio of water film thickness to the composite surface roughness. The control equation is expressed as follows [33]:

$$\frac{\partial}{R_B^2\partial\theta}\left(\phi_\theta\frac{\rho h^3}{12\eta}\frac{\partial p_h}{\partial\theta}\right)+\frac{\partial}{\partial z}\left(\phi_z\frac{\rho h^3}{12\eta}\frac{\partial p_h}{\partial z}\right)=\frac{v_{J\theta}(t)}{2}\left(\phi_c\frac{\partial\rho h}{R_B\partial\theta}+\rho\sigma\frac{\partial\phi_s}{R_B\partial\theta}\right)+\frac{\partial\rho h}{\partial t} \quad (5)$$

where R_B and h are the bearing radius and water film thickness, respectively; z and θ are the circumferential angle ($\theta\in(0, 2\pi)$) and coordinate along the axial direction of the bearing, respectively; ρ and η denote the density and viscosity of the lubricant, respectively; P_h and σ are the hydrodynamic pressure and composite surface roughness, respectively; ϕ_s, ϕ_c represent the shear and contact factors, respectively; and ϕ_θ and ϕ_z indicate the flow factors of the WLB in the circumferential and axial directions, respectively. Each flow coefficient is related to the ratio of the water film thickness to the combined surface roughness and can be determined by the following equation.

$$\begin{cases}\phi_\theta=(h/\sigma,\gamma)=1-Be^{-\tau\left(\frac{h}{\sigma}\right)}\\ \phi_z=(h/\sigma,1/\gamma)\end{cases} \quad (6)$$

$$\phi_s(h/\sigma,\gamma)=\begin{cases}a_1\left(\frac{h}{\sigma}\right)^{\alpha_1}e^{-\alpha_2\left(\frac{h}{\sigma}\right)+\alpha_2\left(\frac{h}{\sigma}\right)^2} & \frac{h}{\sigma}\le 5\\ a_2e^{-0.25\left(\frac{h}{\sigma}\right)} & \frac{h}{\sigma}>5\end{cases} \quad (7)$$

$$\begin{cases}\phi_c=e^{-0.6912+0.782\frac{h}{\sigma}-0.304\left(\frac{h}{\sigma}\right)^2+0.0401\left(\frac{h}{\sigma}\right)^3}, & 0\le\frac{h}{\sigma}<3\\ \phi_c=1, & \frac{h}{\sigma}\ge 3\end{cases} \quad (8)$$

where γ is the surface roughness orientation, which was set to 1 in this study to indicate that the roughness surface is isotropic. The values of the parameters in Equations (6)–(8) can be found in [16,28].

$v_{J\theta}(t)$ denotes the transient speed during the start-up state [15]. This study assumes that the start-up acceleration process follows a linear acceleration process, which can be governed by

$$v_{J\theta}(t)=\frac{v_m t}{t_a}\quad 0\le t\le t_a \quad (9)$$

In Equation (7), v_m and t_a are the final velocity and the accelerating time of the WLB.

2.3.2. Hydrodynamic Forces

The solution of the average Reynolds equation yields the distribution of the dynamic pressure P_h of the water film in the solution domain at each instant of time. And the transient hydrodynamic forces can be obtained by integrating the hydrodynamic pressure, which can be expressed by

$$\begin{cases}F_{h\xi 0}(t)=\int_0^{2\pi}\int_0^{L}R_Bp_h(\theta,z,t)\sin(\theta)dzd\theta\\ F_{h\kappa 0}(t)=-\int_0^{2\pi}\int_0^{L}R_Bp_h(\theta,z,t)\cos(\theta)dzd\theta\end{cases} \quad (10)$$

2.4. 3D Thermal Model

After considering the journal shape error, the transient frictional heat during the start-up of the bearing cannot be neglected [14]. In the numerical calculation of the transient three-dimensional (3D) thermal characteristics of WLBs, the lubricating medium of the WLB and the rigid journal are considered as thermal coupling conductors, considering the transient characteristics of the fluid–solid–thermal multi-field coupling during the start-up stage. Using the Euler method, the transient 3D thermal transfer behaviors of the bearing are governed by

$$\begin{cases} \rho C_P\left[\frac{\partial T}{\partial t}+v_r\frac{\partial T}{\partial r}+v_\theta\frac{\partial T}{r\partial\theta}+v_z\frac{\partial T}{\partial z}\right]=\frac{\partial}{\partial r}\left(k_r\frac{\partial T}{\partial r}\right)+\frac{\partial}{r\partial\theta}\left(k_\theta\frac{\partial T}{r\partial\theta}\right)+\frac{\partial}{\partial z}\left(k_z\frac{\partial T}{\partial z}\right)+\Phi \\ \frac{\partial}{r\partial r}\left(rk_r\frac{\partial T}{\partial r}\right)+\frac{\partial}{r^2\partial\theta}\left(k_\theta\frac{\partial T}{\partial\theta}\right)+\frac{\partial}{\partial z}\left(k_z\frac{\partial T}{\partial z}\right)=0 \end{cases} \tag{11}$$

where C_p represents the specific heat capacity; k_r, k_θ, and k_z are the coefficients of thermal conductivity along the r, θ, and z directions of the WLB, respectively; v_r, v_θ, and v_z indicate the velocity components along the r, θ, and z directions, respectively; $T(T_B,T_W,T_J)$ is the temperature; the subscripts B and J stand for bearings and journals, respectively; the W subscripts represent the lubricating medium water; and the heat source Φ in the mixed frictional contact zone of the bearing contains the heat of viscous shear dissipation Φ_W of the water film shear and the heat of frictional contact Φ_C of the asperity friction. For more information on the thermal model, see [16,34].

Insufficient dynamic pressure and frequent asperity contact of the contact surface lead to higher temperatures in the bearing system, which has an effect on the viscosity. Therefore, the 3D viscosity of the lubricant was evaluated using the following viscosity–temperature relationship:

$$\eta(\theta,z,r)=1.005\times10^{-3}\left(\frac{T_W(\theta,z,r)+273.15}{293}\right)^{8.9}e^{[4700(1/(T_W(\theta,z,r)+273.15))-1/293]} \tag{12}$$

where T_W is the lubricant temperature.

2.5. Transient Contact Model

2.5.1. Transient Asperity Contact

At the beginning of a WLB's operation, the journal and bush contact surfaces may encounter heightened mixed friction behavior, leading to higher contact pressure. This is especially noticeable when the journal has a shape error [25]. Therefore, assuming that the surface topography of the friction pair conforms to a Gaussian distribution, the contact pressure calculation model developed by Kogut and Etsion (KE model) [35], which is able to take into account the complete plastic deformation, is utilized to determine the transient contact pressure under the mixed lubrication stage, and the governing equations are [36]:

$$\begin{aligned} P_c=&\tfrac{2}{3}\pi\sigma\beta DK\omega_c^*\left(\int_{h^*}^{h^*+\omega_c^*}I_c^{1.5}+1.03\int_{h^*+\omega_c^*}^{h^*+6\omega_c^*}I_c^{1.425}\right.\\ &\left.+1.4\int_{h^*+6\omega_c^*}^{h^*+110\omega_c^*}I_c^{1.263}+\tfrac{3}{K}\int_{h^*+110\omega_c^*}^{\infty}I_c^{1}\right)\end{aligned} \tag{13}$$

where D and β are the asperities density and the composite radius of curvature of the asperity, respectively. According to Beheshti's research [37], $\sigma\beta D$ and β/σ are assumed to be 0.04 and 100 in this numerical model, respectively. The superscript '*' indicates that the parameters are dimensionless, and $h^*=\frac{h}{\sigma}$, h^* and ω_c^* are normalized by the composite surface roughness. I_c denotes the integral operation. The calculation equation of I_c and ω_c^* can be found in [31].

2.5.2. Contact Forces

After solving the KE model to obtain the transient contact pressure during the bearing start-up state, the contact forces are determined by

$$\begin{cases} F_{c\xi}(t) = \int_0^{2\pi}\int_0^{L} R_B p_c(\theta,z,t)\sin(\theta)dzd\theta \\ F_{c\kappa}(t) = -\int_0^{2\pi}\int_0^{L} R_B p_c(\theta,z,t)R_B\cos(\theta)dzd\theta \end{cases} \tag{14}$$

2.6. Transient Deformation

In this study, the journal is made of 45-gauge steel and the bush is made of PEEK. The stiffness of the journal is considerably greater than that of the bush. Thus, the journal is assumed to be a rigid isothermal expanding body. According to Equation (1), the total deformation of WLBs can be calculated by

$$\begin{array}{l} \delta_B(\theta,z,t,\Delta T,p) = \delta_{BE}(\theta,z,t,p) + \delta_{BT}(\theta,z,t,\Delta T,p) \\ \delta_J(\theta,r,t,\Delta T,p) = \delta_{JT}(\theta,r,t,\Delta T,p) = \alpha_J \Delta T R_J(1+\varepsilon(t)\cos(\theta(t)-\varphi)) \end{array} \tag{15}$$

where α_J and R_J indicate the thermal expansion and radius of the journal, respectively, and the thermal deformation and elastic deformation are solved by the influence coefficient method [38].

$$\begin{cases} \delta_{BE}(\theta_i,z_j,t,p) = \sum_{\zeta}\sum_{\kappa} G_{BE}(\theta_i,z_j,\theta_\zeta,z_\kappa) \times \left[p_h(\theta_\zeta,z_\kappa,t) + p_c(\theta_\zeta,z_\kappa,t)\right] \\ \delta_{BT}(\theta_i,z_j,t,\Delta T) = \sum_{\zeta}\sum_{\kappa}\sum_{\lambda} G_{BT}(\theta_i,z_j,\theta_\zeta,z_\kappa,r_\lambda) \times \Delta T(\theta_\zeta,z_\kappa,r_\lambda,t) \end{cases} \tag{16}$$

where G_{BE} and G_{BT} represent the elastic deformation coefficient matrix and heat distortion influence coefficient matrix of the bearing, respectively; and $G_{BE}(\theta_j,z_k,\theta_\zeta,z_\kappa)$ is defined as the normal elastic deformation of the bearing surface produced at node (θ_i,z_j) by the unit force applied at node (θ_ζ,z_κ) to the bush surface. The coefficient influence of thermoelastic deformation is calculated using the finite element method (FEM) [39].

2.7. Transient Friction Forces

The effect of transient friction on the transient tribo-dynamic behavior of WLBs during the start-up state is considerable. During the start-up of WLBs, transient friction is determined by the transient shear stress of the hydrodynamic and the asperity contact, which can be calculated using the following equation.

$$\begin{cases} F_{fric\zeta}(t) = \int_0^{L}\int_0^{2\pi}\left(\frac{\eta\omega R_B}{h(t)} + \frac{h(t)}{2}\frac{\partial p_h(t)}{R_B\partial\theta} + \mu_c p_c(t)\right)\cos(\theta)d\theta dz \\ F_{fric\kappa}(t) = \int_0^{L}\int_0^{2\pi}\left(\frac{\eta\omega R_B}{h(t)} + \frac{h(t)}{2}\frac{\partial p_h(t)}{R_B\partial\theta} + \mu_c p_c(t)\right)\sin(\theta)d\theta dz \end{cases} \tag{17}$$

where μ_c denotes the boundary friction coefficient.

2.8. Boundary Conditions

2.8.1. Thermal Boundary

As shown in Figure 3, the following three types of thermal boundary conditions are used in this study to better simulate the fluid–solid–thermal coupling characteristics of the WLB system:

(a) Internal heat exchange boundary conditions (BC1-BC2);
(b) External heat exchange boundary conditions (BC3-BC8);
(c) Cavitation boundary conditions.

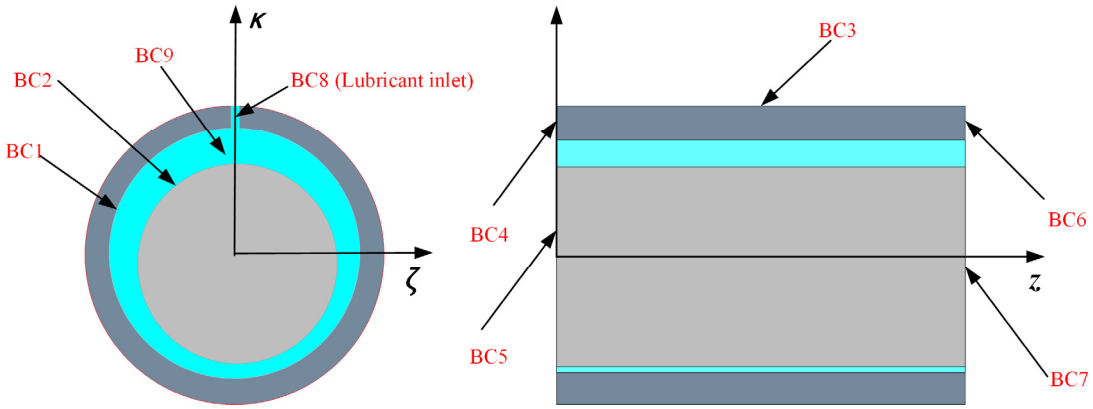

Figure 3. Schematic diagram of thermal boundary conditions of WLBs.

In the water film rupture region (near BC9, shown above), the water film temperature is evaluated using a cavity boundary condition, which can be controlled by

$$\frac{1}{\varsigma} = \frac{(1-\psi)}{\varsigma_g} + \frac{\psi}{\varsigma_l} \tag{18}$$

where ς is related to the lubricant viscosity, specific heat capacity, and heat transfer coefficient; and ψ is equal to the ratio of h_{rup} and h, where h_{rup} and h represent the rupture film thickness and the standard film thickness, respectively.

The interested reader is referred to [37] for more information on thermal modeling.

2.8.2. Cavitation Boundary

Vincent et al. [40] performed a numerical analysis of the performance of journal bearings and concluded that the use of Reynolds boundary conditions can yield accurate hydrodynamic predictions. Consequently, this model incorporates Reynolds boundary conditions to account for cavitation effects in the bearing circumferential direction during simulation calculations, which are described as

$$\begin{cases} p_h(\theta, 0) = 0 \\ p_h(\theta, L) = 0 \\ p_h(\theta_0, z) = 0 \\ \partial p_h(\theta_0, z)/\partial\theta = 0 \end{cases} \tag{19}$$

where θ_0 and L represent the location of the water film rupture and length of the bearing, respectively.

3. Numerical Schemes

3.1. Numerical Scheme of the Reynolds Equation

To satisfy the fluid mass conservation condition, this study assumes that the fluid flowing into and out of the computational cell is equal. Thus, the Reynolds equation is discretely solved using the control volume method (CVM) [2]. A schematic diagram of the nodes of the control cell is given in Figure 4. Based on this, the average Reynolds equation (Equation (6)) can be discretized as

$$\begin{aligned} &\left[\left(\frac{1}{R^2}\phi_\theta\frac{\rho h^3}{12\eta}\frac{\partial p_h}{\partial\theta}\right)_e - \left(\frac{1}{R^2}\phi_\theta\frac{\rho h^3}{12\eta}\frac{\partial p_h}{\partial\theta}\right)_w\right]\Delta\theta_{j,k} + \left[\left(\phi_z\frac{\rho h^3}{12\eta}\frac{\partial p_h}{\partial z}\right)_n - \left(\phi_z\frac{\rho h^3}{12\eta}\frac{\partial p_h}{\partial z}\right)_s\right]\Delta z_{j,k} \\ &= \frac{\omega(t)\phi_c}{2}[(\rho h)_e - (\rho h)_w]\Delta\theta_{j,k} + \frac{\omega(t)\rho\sigma}{2}[(\phi_s)_e - (\phi_s)_w]\Delta\theta_{j,k} + \frac{\partial\rho h}{\partial t}\Delta\theta_{j,k}\Delta z_{j,k} \end{aligned} \tag{20}$$

where $\Delta\theta_{j,k}$ and $\Delta z_{j,k}$ denote the mesh size of the control volume (j, k), respectively. Equation (24) can be simplified in terms of the interface node coefficients, K, for the control volume in each direction.

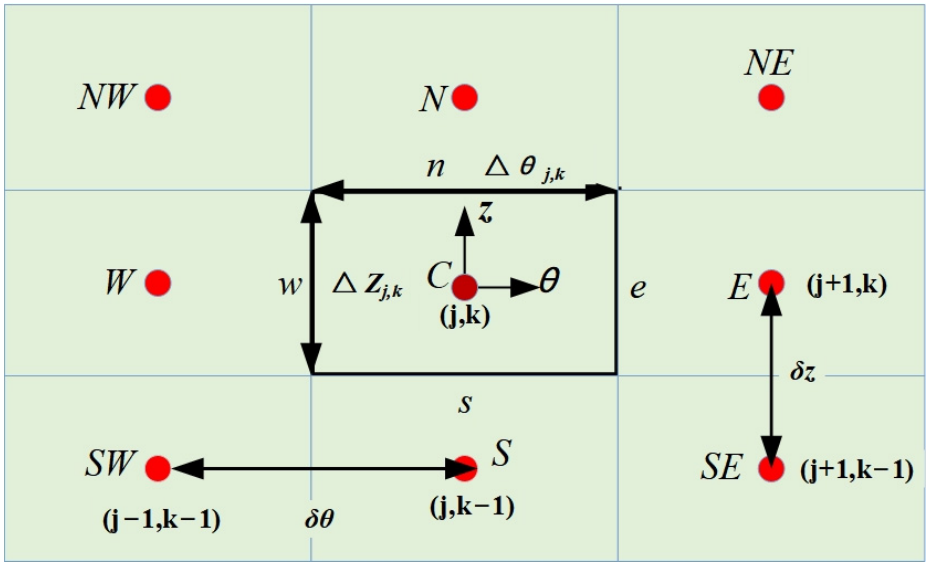

Figure 4. Nodal schematic of the control volume method.

After processing, the final discrete Reynolds equation can be organized in the following form.

$$A_N p_{h,N} + A_S p_{h,S} + A_E p_{h,E} + A_W p_{h,W} + A_C p_{h,C} = B_P \tag{21}$$

Details of the discretization process for the Reynolds equation can be found in [31].

Subsequently, the resulting discrete Reynolds equations are computed iteratively using the successive over relaxation (SOR) method. During each iteration, the hydrodynamic pressure is updated by the following equation:

$$p_{h,C}^{(new)} = (1-\psi)p_{h,C}^{(old)} + \psi\bar{\bar{p}}_{h,C}^{(new)} \tag{22}$$

where ψ is the over-relaxation factor, which was given as 1.5 in this model.

When the hydrodynamic pressure of the current iteration satisfies the following equation, the iterative calculation stops and the hydrodynamic pressure at this point is output.

$$\frac{\sum_{j=1}^{n}\sum_{k=1}^{m}\left|p_{j,k}^{(new)} - p_{j,k}^{(old)}\right|}{\sum_{j=1}^{n}\sum_{k=1}^{m}\left|p_{j,k}^{(old)}\right|} \le 1.0\times10^{-6} \tag{23}$$

3.2. Numerical Scheme of the Dynamic Equation

In this study, the journal dynamics equations (Equation (5)) were calculated iteratively using the Newmark method to obtain the journal trajectories under the interaction of forces and static load. The control equations for the iterative computational process are:

$$\begin{cases} \zeta\prime_{t+\Delta t}(t) = \zeta'_t + \left[(1-\alpha)\zeta''_t + \alpha\zeta''_{t+\Delta t}\right]\Delta t \\ \zeta_{t+\Delta t}(t) = \zeta_t + \zeta\prime_t\Delta t + \left[(1/2-\beta)\zeta''_t + \beta\zeta''_{t+\Delta t}\right]\Delta t^2 \\ \kappa\prime_{t+\Delta t}(t) = \kappa'_t + \left[(1-\alpha)\kappa''_t + \alpha\kappa''_{t+\Delta t}\right]\Delta t \\ \kappa_{t+\Delta t}(t) = \kappa_t + \kappa'_t\Delta t + \left[(1/2-\beta)\kappa''_t + \beta\kappa''_{t+\Delta t}\right]\Delta t^2 \end{cases} \tag{24}$$

where ζ, ζ', ζ'' and $\kappa, \kappa', \kappa''$ are the displacements, velocities, and accelerations of the journal, respectively. Δt is the time step during the iteration. α and β are the constants, which were set as 0.5 and 0.25, respectively.

The convergence criterion for 3D temperature is shown below.

$$\frac{\left|T_{max}^{(old)} - T_{max}^{(new)}\right|}{\left|T_{max}^{(old)}\right|} \leq 1.0 \times 10^{-6} \tag{25}$$

The solution process of the start-up tribo-dynamic model of the fluid–solid–thermal multi-field coupling WLB, considering the journal shape error, includes the steady-state process and transient process, as shown in Figure 5. Before starting the calculation, the asperities contact pressure at the initial time needs to be determined and used as an initial parameter for the transient tribo-dynamics. In the solution process of a transient tribo-dynamics model, the most critical step lies in how to realize the time-varying parameter mapping between the journal dynamics equations and the transient fluid–solid–thermal lubrication model of the bearings. This study utilizes the transient hydrodynamic forces, contact forces, and mixing friction obtained by solving the transient fluid–solid–thermal lubrication model at the current time step t as inputs for the journal dynamics equations. The dynamics equations are then solved to obtain the transient displacement at the journal center. This transient displacement is then coupled with the transient elastic deformation, thermal deformation (bearing and journal), and journal shape error to update the transient lubrication gap at the next time step $t + \Delta t$. Thus, the fluid–solid–thermal coupling characteristics of the bearings under the start-up condition are realized.

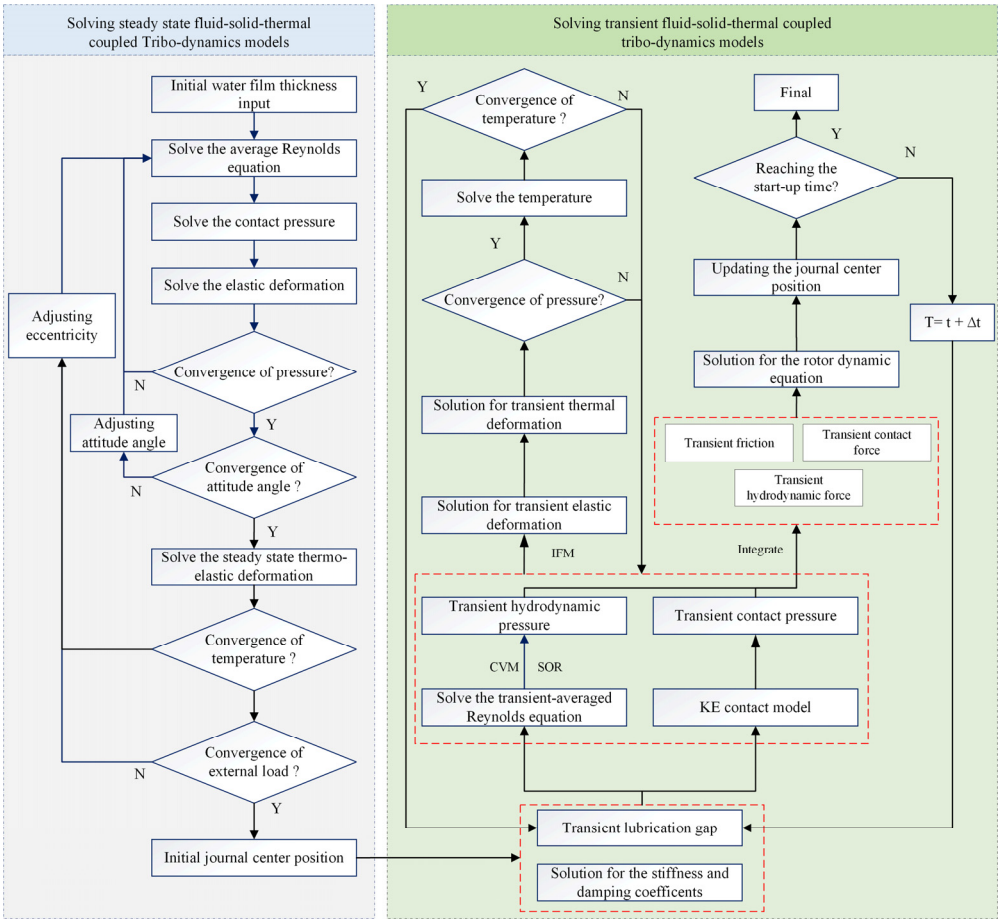

Figure 5. Solution flow of numerical model for start-up state of water lubrication.

4. Results and Discussion

4.1. Verification of Present Model

The effect of journal shape error on the start-up behavior of WLBs in this model was sufficiently verified in [31]. Therefore, this content will not be verified in this study. The simulation results of the temperature rise during start-up predicted by the established coupled fluid–solid–thermal model were compared with the experimental results provided by Kucinschi [41]. From Figure 6, it can be found that the temperature distribution of the bushing–film interface and the shaft–film interface on the circumference of the journal bearing at different operation times is in general agreement with the test results of Kucinschi et al. [41]. Thus, these validation results demonstrate that the developed model can effectively predict the thermal performance of journal bearings during the start-up state. The test parameters used in [41] are shown in Table 1. It is worth noting that Kucinschi's experiments did not consider journal shape errors.

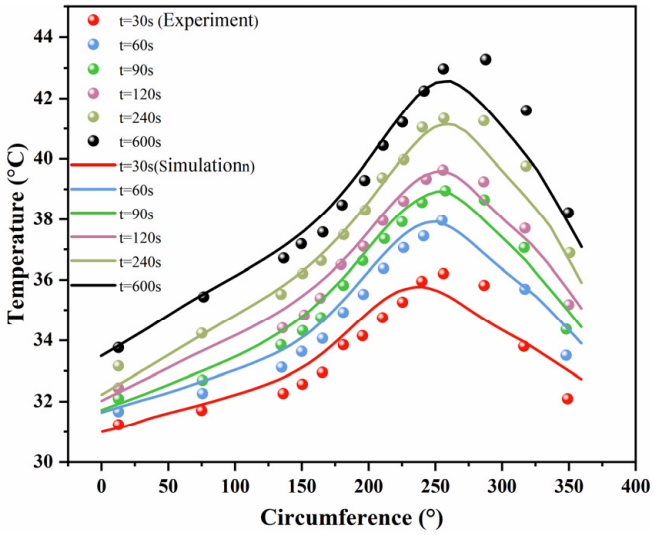

Figure 6. Verification of radial bearing transient circumferential temperature distribution during start-up state.

Table 1. Kucinschi's experimental parameters [41].

Parameter	Value	Parameter	Value
Bearing radius	50 mm	Bearing width	80 mm
Bearing specific heat capacity	380 J/(kg·K)	Journal specific heat capacity	490 J/(kg·K)
Radius clearance	0.123 mm	Lubricant specific heatcapacity	2000 J/(kg·K)
Journal thermal expansivity	12 μm/(m·K)	Bearing thermal expansivity	17 μm/(m·K)
Bearing Poisson ratio	0.3	Bearing elastic modulus	120 GPa
Journal elastic modulus	210 GPa	lubricating temperature	30 °C
Journal Poisson ratio	0.33	Lubricant viscosity (30 °C)	0.05 Pa·s
Bearing thermal conductivity	65 W/m·K	Journal thermal conductivity	50 W/m·K
Bearing density	8940 kg/m^3	Journal density	7700 kg/m^3
Lubricant thermal conductivity	0.13 W/m·K	Lubricant density	870 kg/m^3
Start-up time	7 s		

4.2. Setting of Simulation Parameters

In this study, the simulation parameters of the tribo-dynamics characteristics of WLBs during the start-up state are shown in Table 2. The journal was rated for 1000 rpm with

a load of 450 N. At t = 0 s, the journal was static. The journal reached its rated operating speed (1000 rpm) at t = 2 s and remained there.

Table 2. Start-up simulation parameters for WLBs.

Parameter	Value	Parameter	Value
Inner radius/R_B	22.5 mm	Water specific heat capacity/C_{PW}	4200 J/(kg·K)
Outer radius/R_O	24 mm	Journal density ρ_J	7800 kg/m^3
Bearing width/L	20 mm	Journal elastic modulus/E_J	210 GPa
Radius clearance/C	0.06 mm	Journal Poisson ratio/ν_J	0.3
Bearing elastic modulus/E_B	3.89 GPa	Journal thermal conductivity/k_J	50 W/(m·K)
Bearing Poisson ratio/ν_B	0.4	Journal specific heat capacity/C_{PJ}	460 J/(kg·K)
Bearing density/ρ_B	1300 kg/m^3	Journal thermal expansivity	11.9 μm/(m·K)
Bearing thermal conductivity/k_B	11 W/(m·K)	Convection heat transfercoefficient/h_h	80 W/(m·K)
Bearing specific heat capacity/C_{PJ}	1005 J/(kg·K)	Inlet temperature/T_{inlet}	20 °C
Bearing thermal expansivity	50 μm/(m·K)	Water thermal conductivity/k_W	0.599 W/(m·K)
Water density/ρ_W	1000 kg/m^3	Journal surface roughness/σ_J	0.2 μm
Water viscosity/η_W	0.001 Pa·s	Bearing surface roughness/σ_B	1.6 μm

4.3. Effect of Different Journal Shape Error Amplitude

Because machining errors and operating wear are inevitable, the presence of journal shape error is unavoidable. This section discusses the effect of the amplitudes of different journal shape errors on the lubrication performance and dynamic response during the start-up of WLBs. Figure 7 shows that there are fluctuating transient hydrodynamic and contact forces when journal shape error is taken in account. This is due to the fact that periodic shape error cause oscillations in the water film, which leads to fluctuations in the mixed lubrication performance of the bearing. When Δr = 0.002–0.009, as shown in Figure 7b, the effect of shape error amplitude on the transient mixed lubrication behavior of the bearing is insignificant compared to the ideal journal. As shown in Figure 7a (Δr = 0.02–0.09), the fluctuations in forces grow in magnitude during start-up as the amplitude of the shape error increases further. In addition, it is obvious that the journal shape error alternately positively and negatively affects the lubrication performance of WLB, as illustrated in Figure 7a. The impact of alternating positive and negative effects is similar to the results when thermal effects are not considered [31].

To investigate the influence of thermal effects on the starting characteristics of the bearings in the presence of journal shape errors, the transient responses of the bearings with and without the considered thermal effects are compared in Figure 8. As indicated in Figure 8a, the thermal effect slightly reduces the overall contact force and maximum contact pressure at the bearing end (by 0.1 MPa). The contact force reduction is more significant with increasing start-up time. This is due to the fact that, as the bearing starts up, the bush thermal deformation continues to increase, making the thermal deformation increase and leading to a decrease in the minimum water film thickness, which in turn increases the dynamic pressure effect and decreases the contact behavior, as shown in Figure 8b. The journal trajectory graph shown in Figure 8c also shows that the thermal effect increases the dynamic pressure effect, causing the journal trajectory to rise.

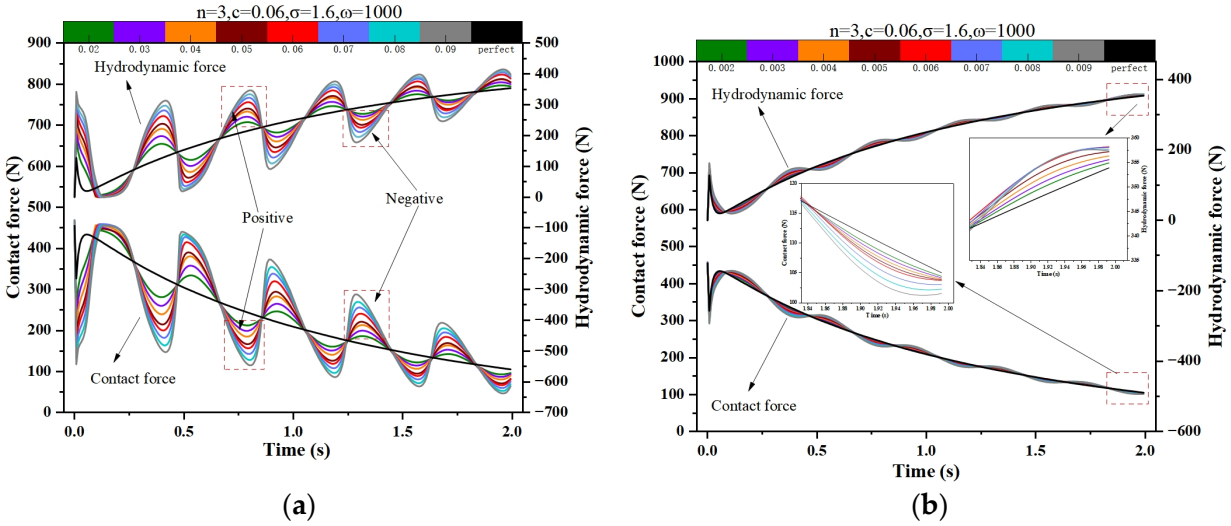

Figure 7. Effect of journal shape error amplitude on transient contact force and transient hydrodynamic force of water-lubricated bearing: (**a**) Δr = 0.02–0.09; (**b**) Δr = 0.002–0.009.

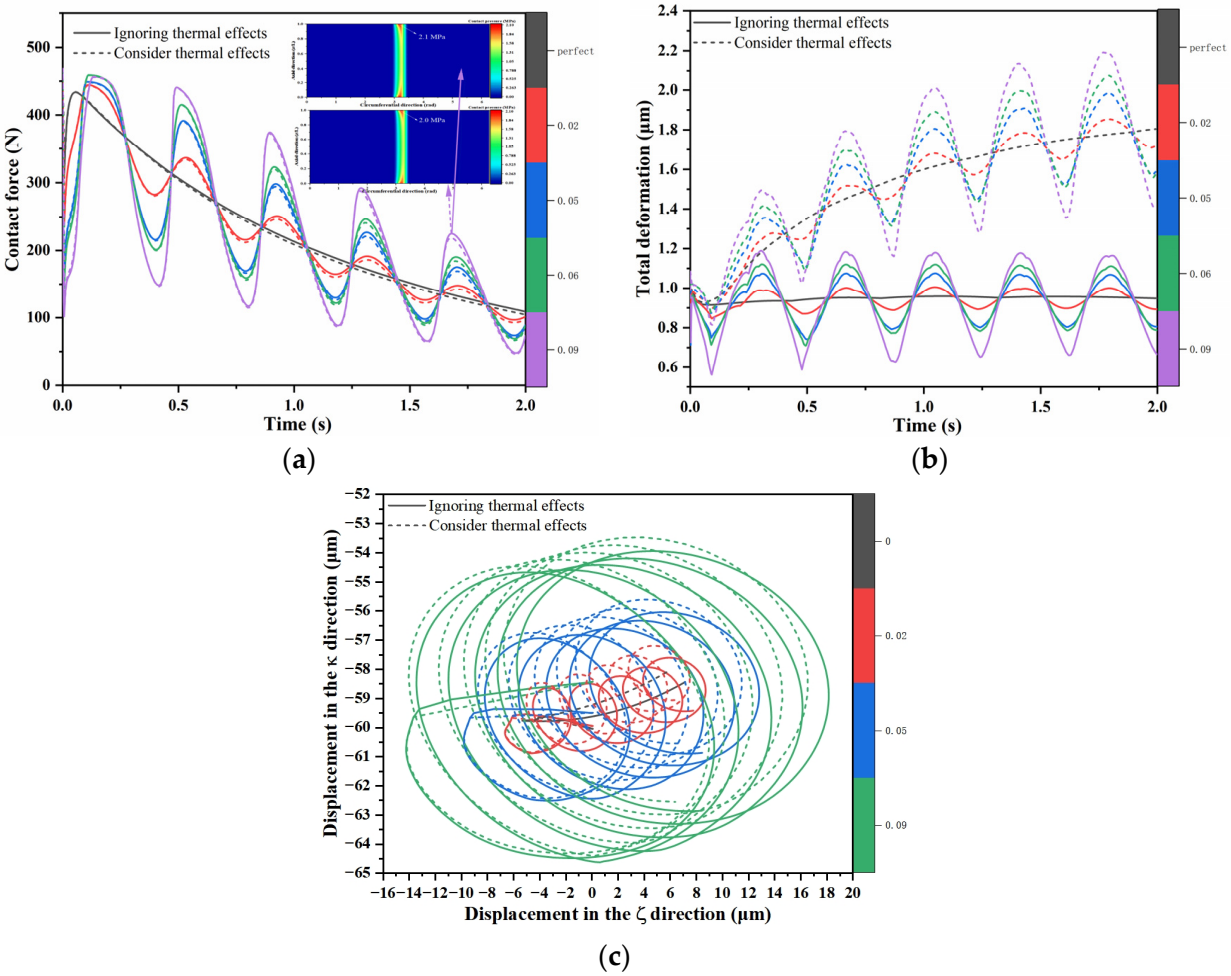

Figure 8. Comparison of dynamic characteristics of bearings with and without consideration of thermal effects: (**a**) contact force; (**b**) deformation; (**c**) journal trajectory.

Figure 9 illustrates the influences of different journal shape error amplitudes on the maximum temperature during start-up of the WLB. The bearing produces more asperity contact friction behavior due to the journal shape error contributing to an increased rise in

temperature in the bearing compared to perfect journals, especially in the range of 2–9% error amplitude. The temperature variation caused by the error amplitude of the journal shape is up to 1.15 °C higher than that due to the perfect journal, and the difference in temperature is proportional to the error amplitude. The presence of journal shape errors has a negative effect on the temperature rise of WLBs, as shown in Figure 9, with overall temperature fluctuations of 2 °C or less. The larger the journal shape error, the more frequent the contact between the contact interface of the bush and journal in the unit time of the start-up process and the more significant the contact behavior, which leads to higher temperatures. As shown in Figure 10, although the larger the error amplitude of the journal shape is, the larger the temperature rise is during start-up state of bearing, the maximum temperature location remains essentially constant in the circumferential direction. That is, the error amplitude of the journal shape does not change the position of the maximum temperature.

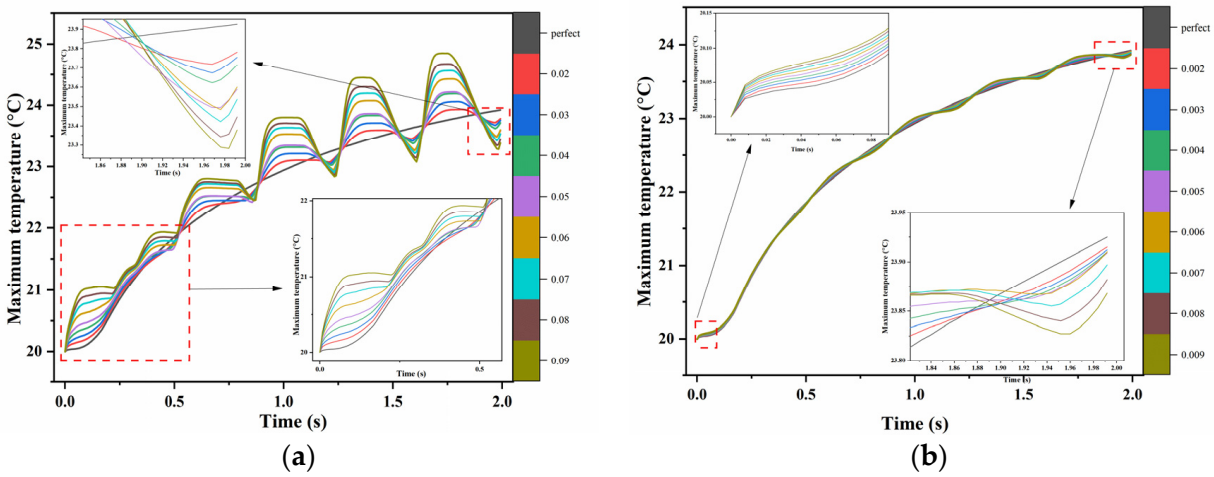

Figure 9. Effect of journal shape error amplitude on transient maximum temperature of the WLB: (**a**) Δr = 0.02–0.09; (**b**) Δr = 0.002–0.009.

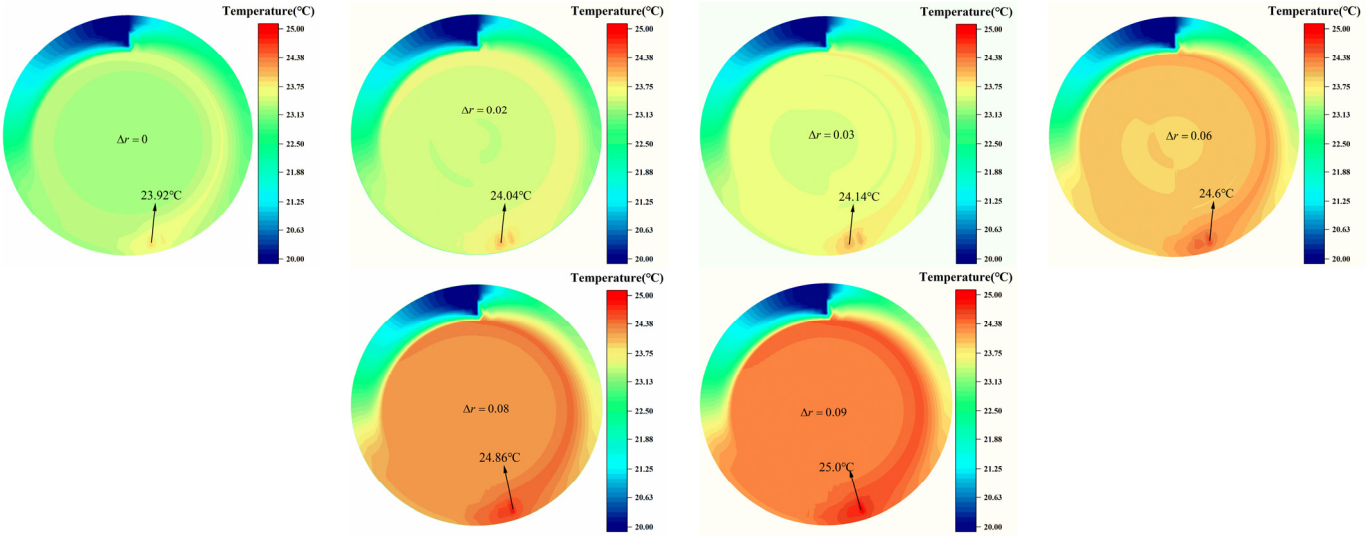

Figure 10. The temperature distribution for different journal shape error amplitudes (within 2 s startup time).

4.4. Effect of Different Journal Shape Error Waviness Orders

This section analyzes how the waviness order in shape error impacts the transient performance of bearings. Figure 11 clearly illustrates the transient dynamical forces under the effect of even-order waviness (Figure 11a) and odd-order waviness (Figure 11b) during

the start-up of bearings. It is evident that fluctuations caused by the waviness order are periodic, with the former differing from the latter by one cycle. Figure 11a shows that the contact and hydrodynamic force exhibit volatility as a result of the journal shape waviness, and the amplitude of the fluctuation decreases as the waviness order decreases. The transient contact hydrodynamic force under the 2nd- and 4th-order journal shape waviness shows a decreasing trend in the range of fluctuation with the increase in the start-up time, while the fluctuation of the 6th, 8th, and 10th order journal shape waviness is larger. As depicted in Figure 11b, odd-ordered waviness generates a larger transient hydrodynamic force during start-up compared to even-ordered waviness. This results in a rapid reduction in friction between the WLB and the journal, positively affecting the bearing's start-up. However, this effect fluctuates with increasing start-up time and gradually disappears as the journal shape waviness order increases further. In addition, the lubrication performance exhibits fluctuation convergence characteristic when the waviness order of the journal shape error in low-priced.

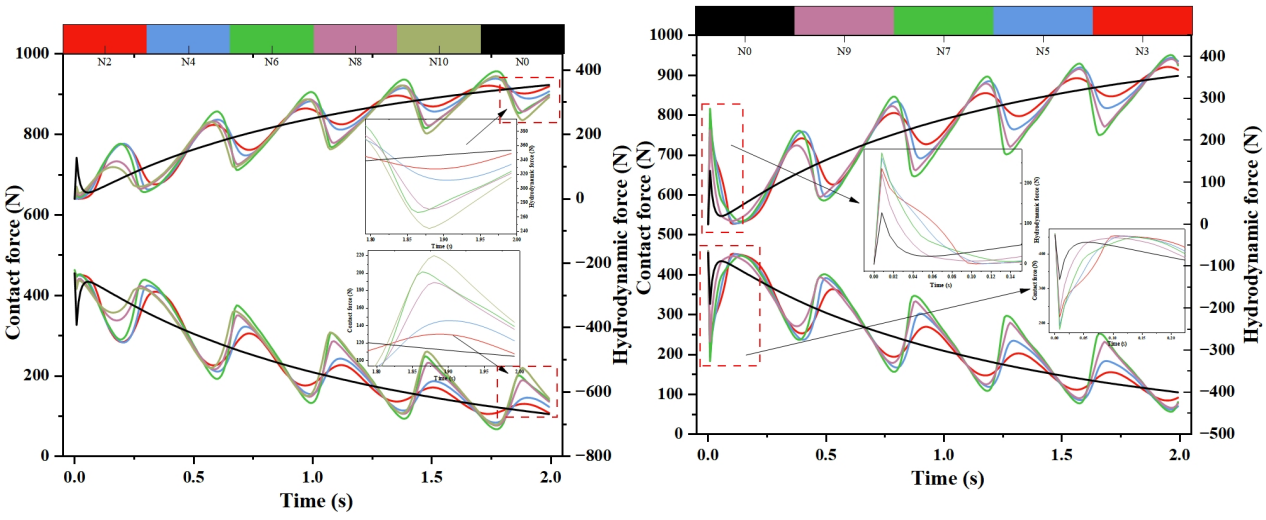

Figure 11. Influence of journal shape error order on transient contact force and transient hydrodynamic force of water-lubricated bearing ($\Delta r = 0.033$): (**a**) even-order; (**b**) odd-order.

Figure 12 demonstrates the impact of temperature on hydrodynamic pressure for shape errors with different waviness orders. The results clearly indicate that the transient hydrodynamic pressure increases when the temperature effect is taken into account. Additionally, the distribution plot shows a slight increase in the dynamic pressure region and the maximum hydrodynamic pressure due to the temperature effect.

Figure 13 confidently displays the journal displacements considered to have odd- and even-order waviness at start-up. As can be seen in Figure 13, compared with the ideal journal, the fluctuation amplitude of the journal trajectory increases and then decreases with the waviness order, with the minimum fluctuation amplitude of the even order being $n = 2$ and the maximum fluctuation amplitude being $n = 8$ and the minimum fluctuation amplitude of the odd order being $n = 3$ and the maximum fluctuation amplitude being $n = 7$. Compared to the ideal journal, the fluctuation amplitude in the κ direction is inversely proportional to the increasing waviness order, with the minimum fluctuation amplitude at $n = 10$ and the maximum fluctuation amplitude at $n = 2$ for even orders and the minimum fluctuation amplitude at $n = 9$ and the maximum fluctuation amplitude at $n = 3$ for odd orders, as illustrated in Figure 13c,d. This is because the κ direction is the primary direction of bush deformation. When the waviness order of the journal shape error is low, the thermal deformation is not significant. Thermal deformation becomes more significant as

the waviness order of the journal shape error increases, resulting in a decrease in vertical displacement during the start-up state of the bearing.

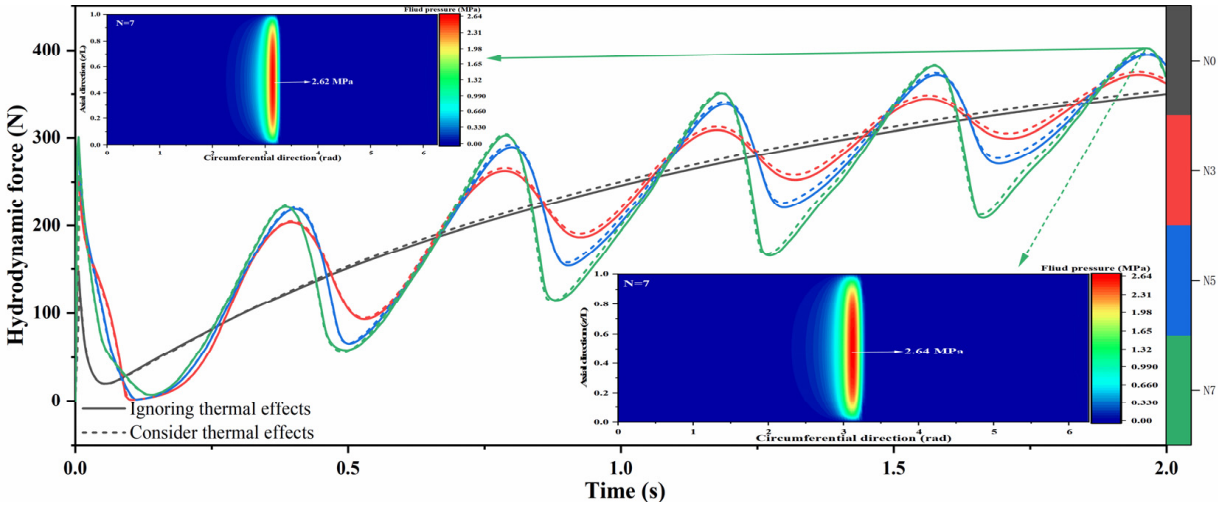

Figure 12. Temperature effects on hydrodynamic pressure for shape errors with different waviness orders.

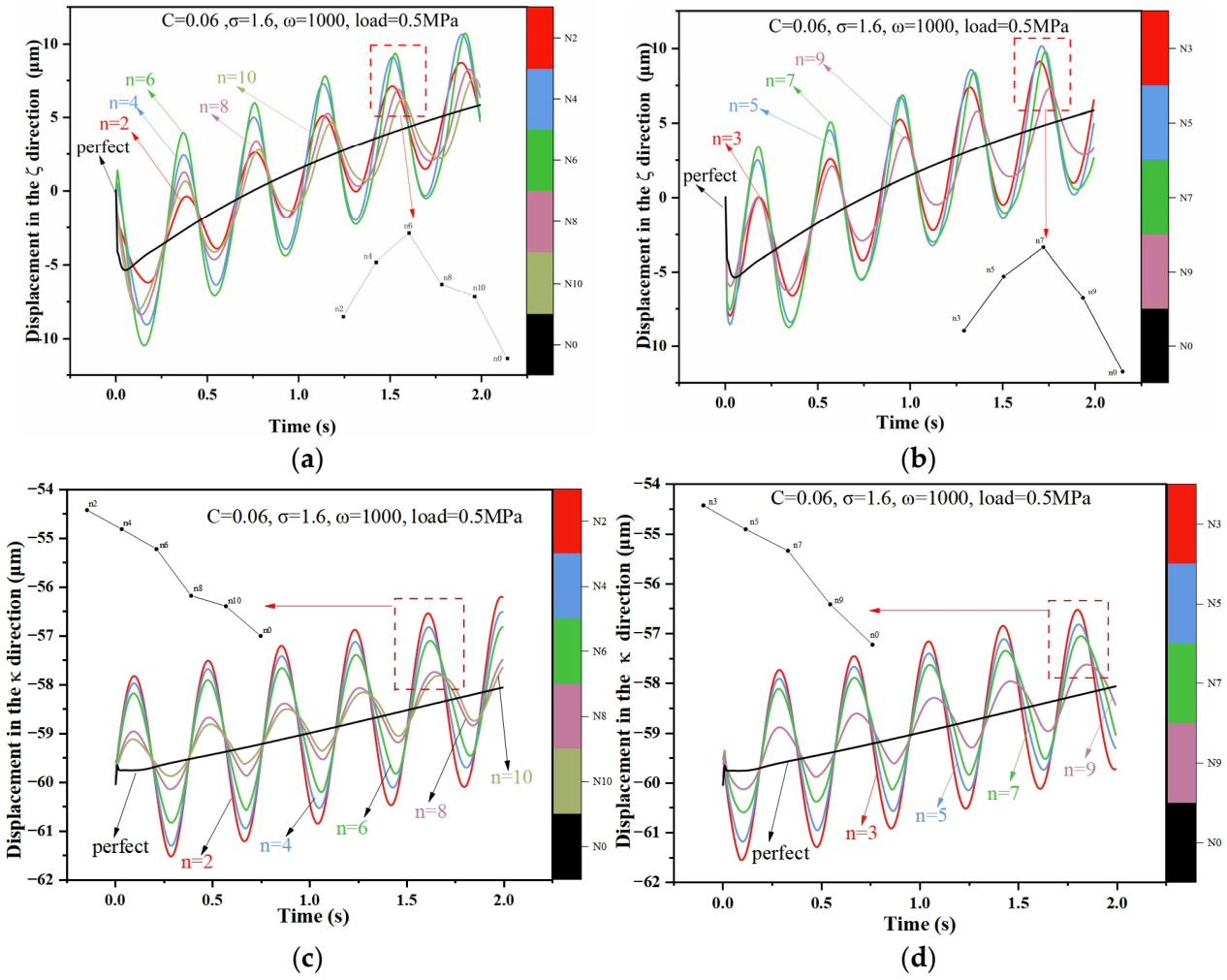

Figure 13. The influence of shape error waviness order on the axis locus of WLBs: (**a**,**c**) even order; (**b**,**d**) odd order; (**a**,**b**) in the ζ direction; (**c**,**d**) in the κ direction.

Figure 14 illustrates the effect of the waviness order of the journal shape error on the transient maximum temperature of WLBs at start-up. As shown in Figure 14, the influence of journal shape error on the transient temperature rise of the WLB is evident at the initial stage of start-up, i.e., before t < 0.5 s. The higher waviness order has a more negative impact on the start-up temperature compared to the ideal journal as the start-up time increases. The overall fluctuation pattern of the instantaneous maximum temperature follows a trend of first increasing and then stabilizing with the waviness error. This may be due to the fact that the start-up process is mainly in a mixed lubrication state, and the journal shape waviness error becomes the main factor affecting the contact. The higher the wave order of the journal, a more dramatic undulation of the journal shape, establishment of the dynamic pressure area of the water film, and destruction of alternating occur, destroying the continuity of the water film. Therefore, it cannot form an effective lubrication, the interface contact behavior is intensified, and the thermal deformation will be more obvious. From Figure 14, it can be seen that, for even-order waviness, the smallest temperature fluctuation amplitude is exhibited at n = 2, and n = 10 exhibits the highest instantaneous maximum temperature (25.37 °C). Odd-order waviness exhibits the highest transient maximum temperature at n = 7 with 25.32 °C. Combined with the above analysis, tin terms of lubrication performance of WLBs, low-order waviness of the shape error is more favorable.

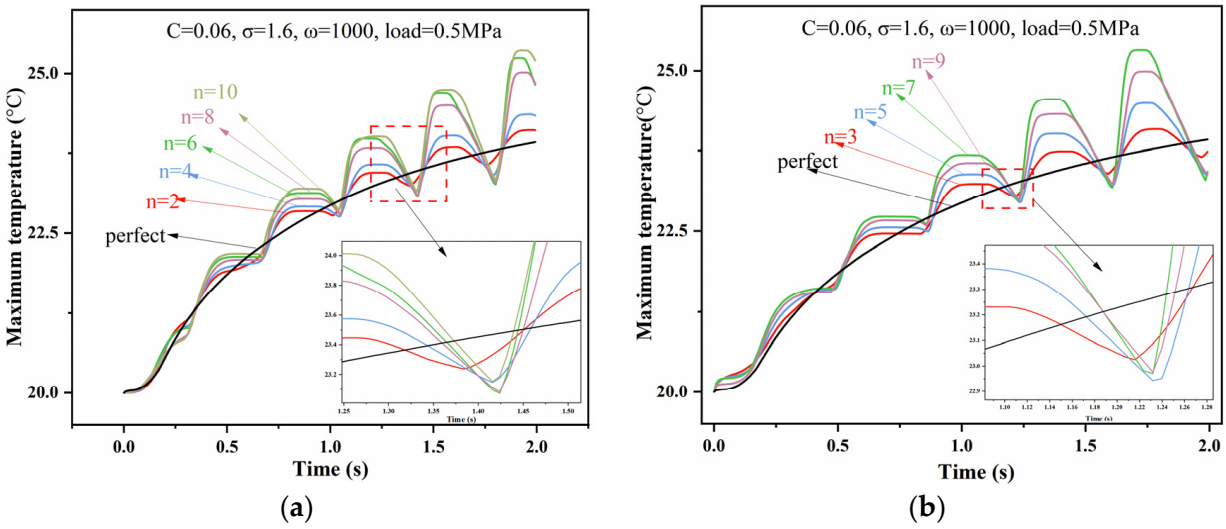

Figure 14. Influence of journal shape error order on transient maximum temperature of water-lubricated bearing: (**a**) even order; (**b**) odd order.

Figure 15 shows the evolution of the transient contact behavior of WLBs for different waviness orders during start-up. As shown in Figure 15a, the contact pressure distribution at 0 s indicates that the contact pressure increases gradually with the increase in the waviness order, which may be due to the existence of the journal shape error reducing the contact area between the journal and the bush. When the start-up time is equal to 0.6 s, the contact pressure of even-ordered waviness journal shapes decreases rapidly, and all of them are smaller than those of ideal journals. This may be due to the fact that the waviness of the journal shape facilitates the formation of a water film during the initial start-up state of the bearing. With increasing speed, the formation and rupture cycle of the water film is shortened, and it is not easy to form a stable water film to provide hydrodynamic pressure, so the final contact pressure is instead greater than the ideal journal. Figure 15b indicates that the transient contact pressure of the odd-order waviness is greater than that of the ideal journal at both t = 0 s and t = 0.6 s. At t = 2 s, the contact pressure of most of the odd-order waviness is lower than the pressure of the ideal journal, while the situation is exactly the opposite for the even-order waviness. In addition, the maximum contact pressure should

move from the center of the bushing to the ends, which is in general agreement with the findings of [42].

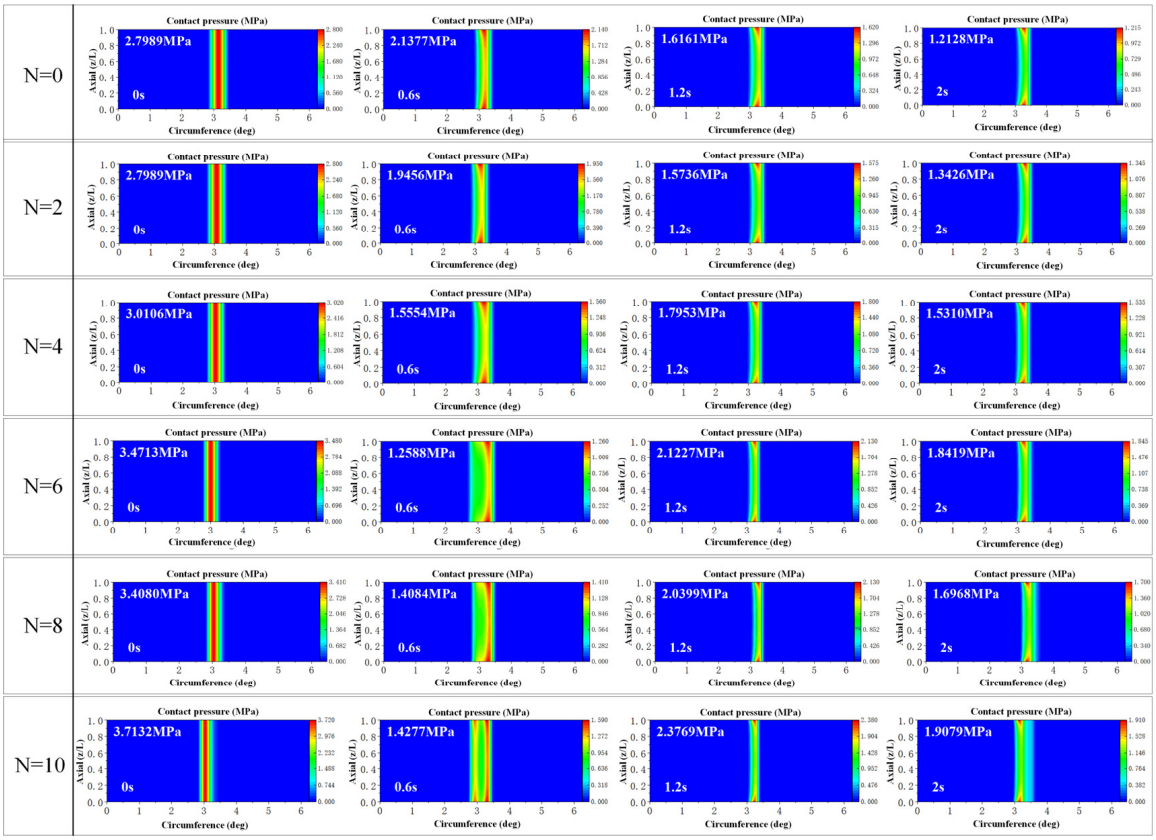

(**a**)

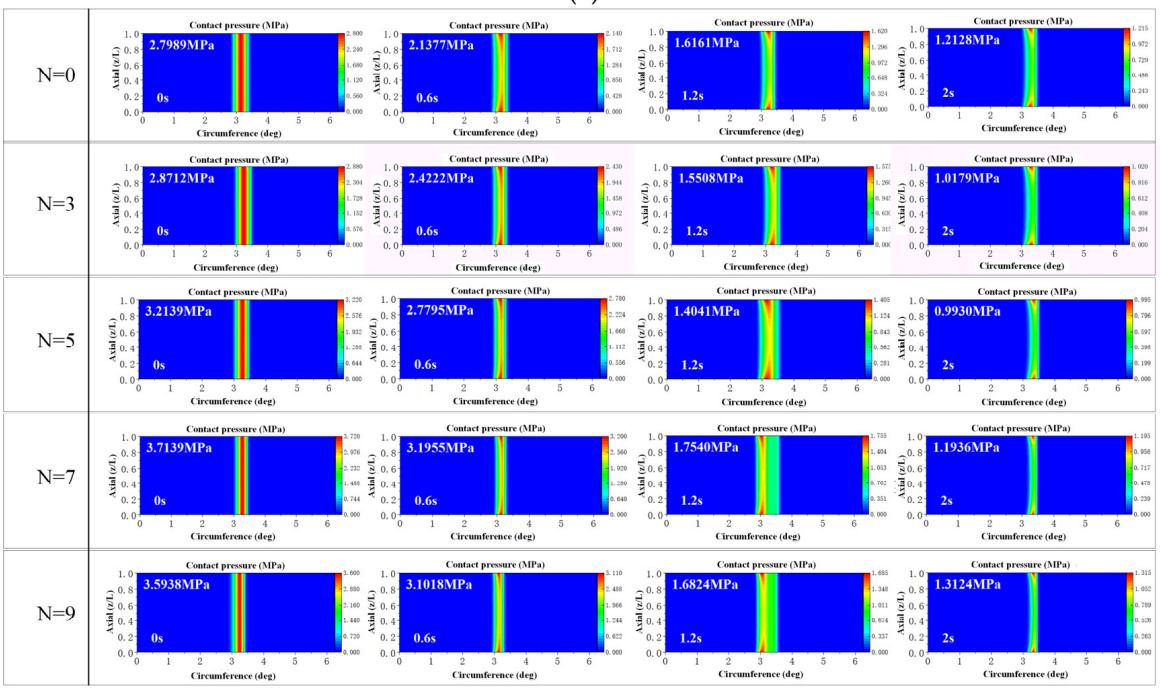

(**b**)

Figure 15. Influence of journal shape error order on transient contact pressure distribution of WLBs: (**a**) even order; (**b**) odd order.

4.5. Effect of Different Starting Speeds on Bearing Performance

The rotational speed is one of the key parameters for the start-up process of WLBs, which directly affects the inertia effect and lubrication status of the journal. This section explores the effect of rotational speed on the performance of bearings during the start-up state under the operating conditions of radius clearance of 0.06, surface roughness of 1.6, and journal shape waviness of the 3rd order with an error amplitude of 0.033%. Figure 16 illustrates the transient contact force time-varying plots for WLBs starting at low and high speeds. The bearing's overall contact forces are significant under low speed. As the start-up time increases, the volatility of the transient contact force gradually decreases. The initial fluctuation amplitude is larger and the fluctuation period is shorter with higher speeds. The fluctuation decay time is proportional to the speed.

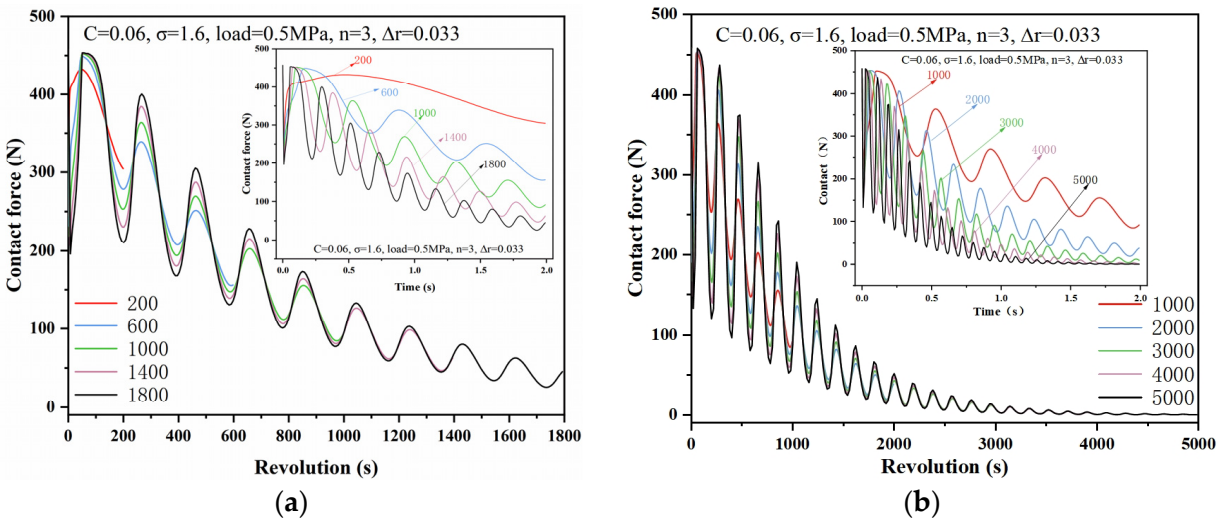

Figure 16. Effect of different rotational speeds on transient contact forces of WLBs at start-up: (**a**) low speed, (**b**) high speed.

Figure 16a demonstrates that the transient contact force of the WLB at the completion of start-up is much larger than 0 N, indicating that the WLB may be operating in boundary lubrication or mixed lubrication. Figure 16b illustrates that the contact force at the completion of the start-up is approximately equal to 0 N when the speed exceeds 3000 rpm. This suggests that the water film may have separated the bush from the journal, and the WLB system is in a state of EHL. Combined with the results of the previous analysis, it can be found that the journal shape error brings fluctuation to the bearing lubrication performance, but does not affect the influence brought by the change in bearing lubrication parameters.

Figure 17 illustrates that neglecting thermal deformation causes the journal displacement to shift towards the lower right. It is important to note that the thermal deformation value resulting from thermal effects is similar to the elastic deformation value resulting from contact, which is approximately 0.8 to 0.9 μm. Taken together with the analytical content of the previous sections, neglecting thermal effects results in an inaccurate calculation of total deformation, leading to an underestimation of the hydrodynamics [14,31]. Furthermore, the prediction of journal displacement would have an error of approximately 1 μm, which is equal to the amount of thermal deformation.

The graph of the bearing temperature variation in the WLBs during the start-up state (Figure 18) shows that the lower the start-up speed, the lower the instantaneous maximum temperature rise in the WLB. When the rotational speed is lower, although the lubrication state of the bearing is worse, the contact frequency and effective friction of the interface of the friction pair at the starting time are much smaller than those at high rotational speed, so the instantaneous maximum temperature rise in the bearing at low speed is lower than that at high speed. From Figure 18b, it can be seen that when the rotational

speed is higher than 2000 rpm, the instantaneous maximum temperature of the bearing first rises to the maximum value and then slowly decreases to a constant value, indicating that the high rotational speed affects the instantaneous temperature rise in the bearing at the starting moment. When the EHL state is reached, its maximum temperature decreases to a constant value as a result of the reduced asperity contact behavior. At the same time, the instantaneous temperature at high speed is much higher than that at low speed, indicating that high speed may cause an instantaneous high temperature rise, thereby increasing the probability of shaft neck locking or burning due to high temperature.

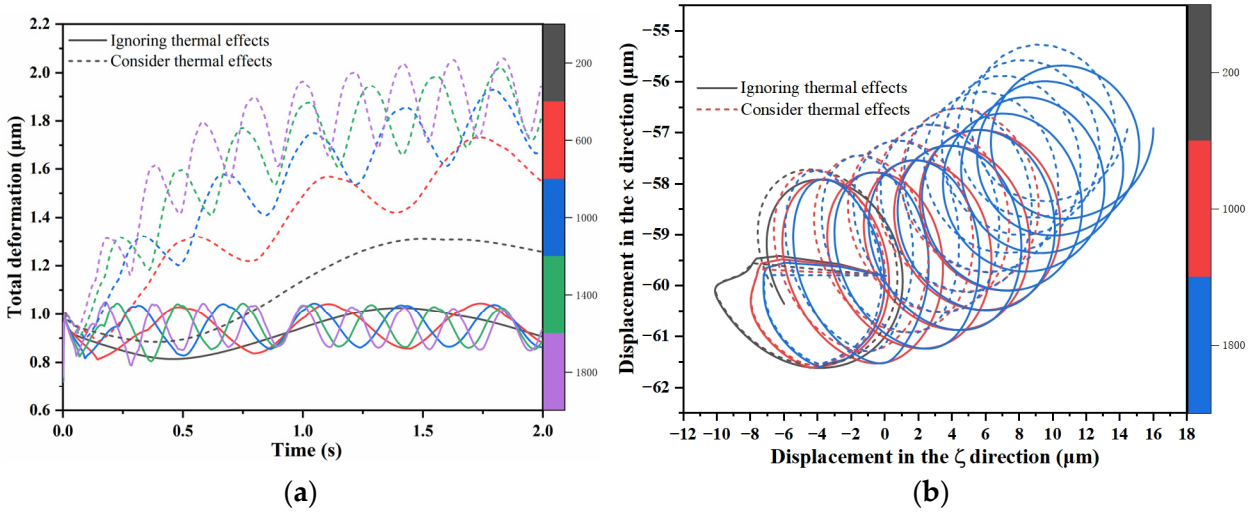

Figure 17. Comparison of dynamic characteristics of bearings with and without consideration of thermal effects: (**a**) deformation; (**b**) journal trajectory.

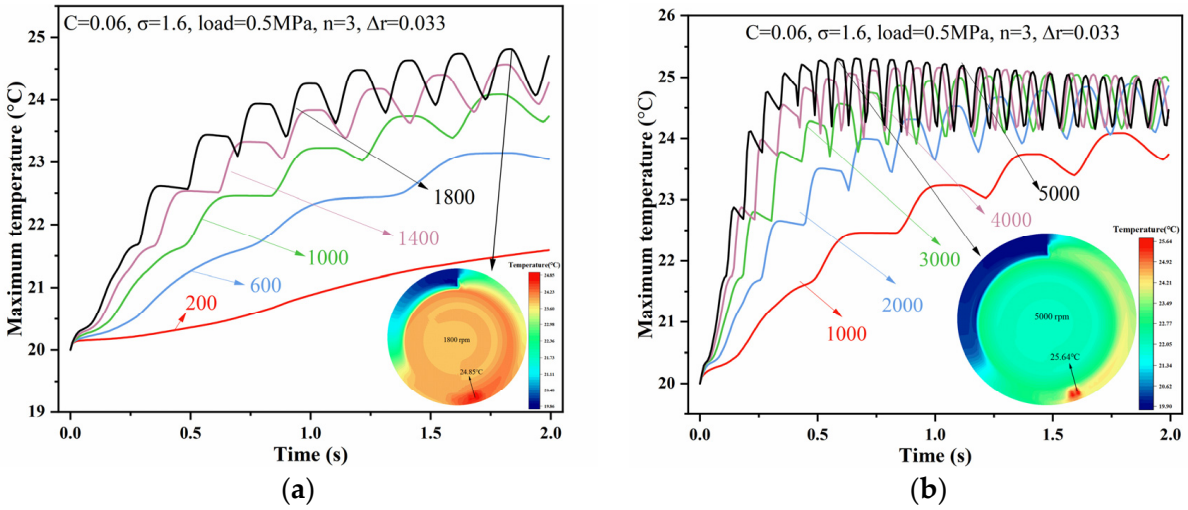

Figure 18. Effect of different rotational speeds on the instantaneous maximum temperature of water-lubricated bearing during start-up: (**a**) low speed, (**b**) high speed.

Figure 19 indicates that the higher the speed, the larger the range of fluctuation in the journal trajectory during start-up, the shorter the displacement fluctuation period, and the more intense the trajectory oscillation. The displacement of the journal in the horizontal direction is greater than that in the vertical direction, which may be due to the presence of static loads along the vertical direction, which can offset some of the transient forces and shock loads generated during the rotation of the journal. While there is no static load in the horizontal direction, nonlinear forces (contact forces, hydrodynamic forces, friction forces), which are susceptible to lubrication gaps, dominate, and therefore, the

displacement fluctuations are rather larger. In addition, the magnitude of the fluctuations the journal trajectories in Figure 19 is basically the same, which suggests that the fluctuation of the displacement may not be related to the rotational speed, but to the journal shape error. The rotational speed mainly affects the fluctuation period of the journal trajectory, and the higher the rotational speed, the shorter the fluctuation period and the larger the displacement. In summary, the results clearly demonstrate that both the shape error of the journal and the starting speed have a significant and undeniable effect on the rise in bearing starting temperature. Furthermore, parameters such as load, radial clearance, and roughness have also been found to have significant impacts on the operating temperature of the bearing [4]. Therefore, further studies are needed to determine the main factors that influence the temperature increase.

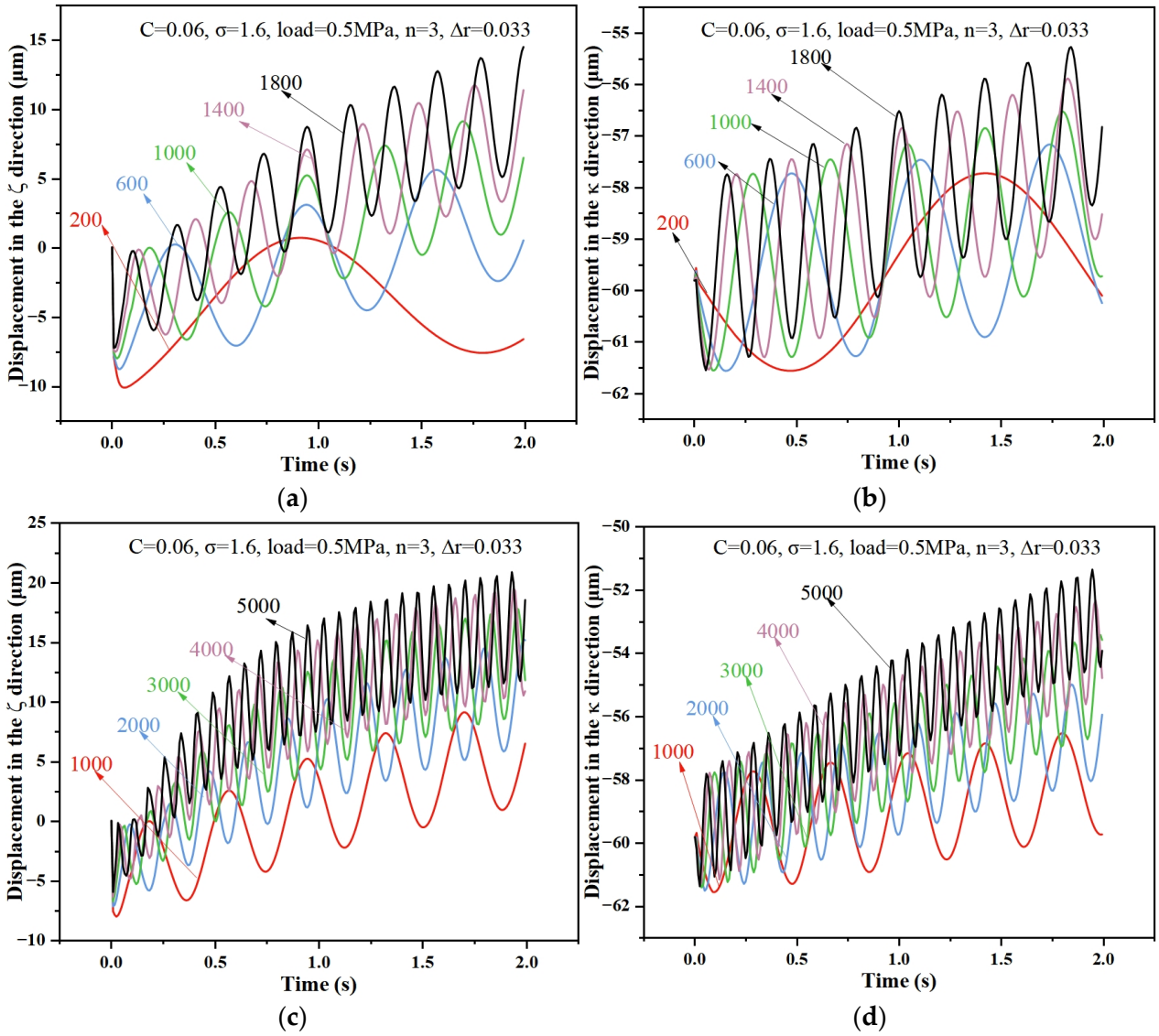

Figure 19. Effects of different rotational speeds on starting journal trajectories of water-lubricated bearings: (**a**) low speed in horizontal direction, (**b**) low speed in vertical direction, (**c**) high speed in horizontal direction; (**d**) high speed in vertical direction.

5. Conclusions

A transient tribo-dynamics model of WLBs considering the fluid–solid–thermal coupling relationship was developed to investigate the effect of journal shape error on the tribo-dynamics behavior during the start-up state. Based on the numerical model after

sufficient validation, the effects of parameters such as the amplitude of journal shape error, waviness order, and rotational speed on the tribo-dynamics characteristics of bearings during start-up were discussed, and the following conclusions were obtained.

(1) The greater the amplitude of the journal shape error, the more pronounced the temperature increase during start-up and the greater the fluctuation in lubrication performance. The location of the maximum temperature during the bearing's start-up state remains unaffected by changes in error amplitude. Temperature changes are not significant when the amplitude of the shape error is less than 9‰ of the bearing radius clearance.
(2) The temperature effect reduces the displacement in the vertical direction during the start-up state of the WLB, which is more significant at higher waviness orders of journal shape error.
(3) The higher the starting speed of the bearing, the easier it is to reach the EHL state, but the temperature rise becomes faster and the shaft track becomes larger. And when the speed is lower, although the temperature is lower, the friction and contact force are greater, so one must be careful when choosing the starting speed.
(4) The neglect of thermal effects leads to an underestimation of the hydrodynamic effect during the startup of WLBs with journal shape errors, resulting in errors in the prediction of the friction dynamics behavior.

Author Contributions: Conceptualization, J.C. and S.C.; methodology, J.C. and S.C.; software, S.C.; validation, J.C. and S.C.; formal analysis, J.C.; investigation, Z.L.; resources, S.C.; data curation, J.C.; writing—original draft preparation, J.C.; writing—review and editing, J.Z. and Z.L.; visualization, J.C.; supervision, J.Z.; project administration, J.Z.; funding acquisition, J.Z. All authors have read and agreed to the published version of the manuscript.

Funding: This research was funded by [Sichuan Science and Technology Program] grant number [24NSFSC0624].

Data Availability Statement: The data that support the findings of this study are available from the corresponding author upon reasonable request.

Acknowledgments: The author(s) disclosed receipt of the following financial support for the research, authorship, and/or publication of this article: This research work was supported by Sichuan Science and Technology Program (Grant No. 24NSFSC0624).

Conflicts of Interest: The authors declare that they have no known competing financial interests or personal relationships that could have appeared to influence the work reported in this paper.

References

1. Zhang, Z.H.; Wang, F.; Wu, X.Y.; Li, C.P. The Influence of Structure Parameters on the Dynamic Pressure Effect of Water-lubricated Journal Bearing. *Hydraul. Pneum. Seal.* **2019**, *39*, 9–14.
2. Xiang, G.; Han, Y.F. Study on the tribo-dynamic performances of water-lubricated microgroove bearings during start-up. *Tribol. Int.* **2020**, *151*, 106395. [CrossRef]
3. Du, Y.Y.; Li, M. Effects on lubrication characteristics of water-lubricated rubber bearings with journal tilting and surface roughness. *Proc. Inst. Mech. Eng. Part J J. Eng. Tribol.* **2020**, *234*, 161–171. [CrossRef]
4. Xie, Z.L.; Jiao, J.; Yang, K.; Zhang, H. A state-of-art review on the water-lubricated bearing. *Tribol. Int.* **2023**, *180*, 108276. [CrossRef]
5. Mokhtar, M.O.A.; Howarth, R.B.; Davies, P.B. Wear characteristics of plain hydrodynamic journal bearings during repeated starting and stopping. *Tribol. Trans.* **1977**, *20*, 191–194. [CrossRef]
6. Mokhtar, M.O.A.; Howarth, R.B.; Davies, P.B. The behavior of plain hydrodynamic journal bearings during starting and stopping. *Tribol. Trans.* **1977**, *20*, 183–190. [CrossRef]
7. Monmousseau, P.; Fillon, M. Transient thermoelastohydrodynamic analysis for safe operating conditions of a tilting-pad journal bearing during start-up. *Tribol. Int.* **2000**, *33*, 225–231. [CrossRef]
8. Cristea, A.F.; Bouyer, J.; Fillon, M. Transient pressure and temperature field measurements in a lightly loaded circumferential groove journal bearing from startup to steady-state thermal stabilization. *Tribol. Trans.* **2017**, *60*, 988–1010. [CrossRef]
9. Krupka, I.; Svoboda, P.; Hartl, M. Effect of surface topography on mixed lubrication film formation during start up under rolling/sliding conditions. *Tribol. Int.* **2010**, *43*, 1035–1042. [CrossRef]

10. Cui, S.H.; Gu, L.; Fillon, M. The effects of surface roughness on the transient characteristics of hydrodynamic cylindrical bearings during startup. *Tribol. Int.* **2018**, *128*, 421–428. [CrossRef]
11. Cui, S.H.; Gu, L.; Wang, L.Q. Numerical analysis on the dynamic contact behavior of hydrodynamic journal bearings during start-up. *Tribol. Int.* **2018**, *121*, 260–268. [CrossRef]
12. Patir, N.; Cheng, H.S. An average flow model for determining effects of three-dimensional roughness on partial hydrodynamic lubrication. *J Tribol.* **1978**, *100*, 12–17. [CrossRef]
13. Greenwood, J.; Tripp, J. The contact of two nominally flat rough surfaces. *Proc. Inst. Mech. Eng.* **1970**, *185*, 625–633. [CrossRef]
14. Xiang, G.; Han, Y.F.; He, T.; Wang, J.X.; Xiao, K.; Li, J.Y. Transient tribo-dynamic model for journal bearings during start-up considering 3D thermal characteristic. *Tribol. Int.* **2020**, *144*, 106123. [CrossRef]
15. Xiang, G.; Wang, C.; Wang, Y.J.; Han, Y.F.; Wang, J.X.; Lv, Z.L. Dynamic Mixed Lubrication Investigation of Water lubricated Bearing with Unbalance Rotor During Start-up. *Tribol. Trans.* **2021**, *64*, 764–776. [CrossRef]
16. Xiang, G.; Yang, T.Y.; Guo, J.; Wang, J.X. Optimization transient wear and contact performances of water-lubricated bearings under fluid-solid-thermal coupling condition using profile modification. *Wear* **2022**, *502–503*, 204379. [CrossRef]
17. Song, M.; Azam, S.; Jang, J.; Park, S.S. Effect of Shape Errors on the Stability of Externally Pressurized Air Journal Bearings Using Semi-Implicit Scheme. *Tribol. Int.* **2017**, *115*, 580–590. [CrossRef]
18. Zhang, H.; Ding, J.G.; Peng, C.; Chang, Y.; Zeng, X.Y.; Yang, H.; Liu, X.B.; Wei, W. Effect of Surface Waviness on the Performances of an Aerostatic Thrust Bearing with Orifice-Type Restrictor. *Int. J. Precis. Eng. Manuf.* **2021**, *22*, 1735–1759. [CrossRef]
19. Cui, H.L.; Wang, Y.; Yue, X.B.; Huang, M.; Wang, W. Effects of Manufacturing Errors on the Static Characteristics of Aerostatic Journal Bearings with Porous Restrictor. *Tribol. Int.* **2017**, *115*, 246–260. [CrossRef]
20. Lee, S.M.; Lee, D.W.; Ha, Y.H.; Lee, S.J.; Hwang, J.H.; Choi, Y.H. A Study on the Influence of Waviness Error to a Hydrostatic Bearing for a Crankshaft Pin Turner. *Tribol. Trans.* **2013**, *56*, 1077–1087. [CrossRef]
21. Rajput, A.K.; Sharma, S.C. Combined Influence of Geometric Imperfections and Misalignment of Journal on the Performance of Four Pocket Hybrid Journal Bearing. *Tribol. Int.* **2016**, *97*, 59–70. [CrossRef]
22. Luboš, S.; Michal, H.; Byrtus, M. Investigation of bearing clearance effects in dynamics of turbochargers. *Int. J. Mech. Sci.* **2017**, *127*, 62–72.
23. Wang, X.; Xu, Q.; Wang, B.; Zhang, L.; Peng, Z. Effect of surface waviness on the static performance of aerostatic journal bearings. *Tribol. Int.* **2016**, *103*, 394–405. [CrossRef]
24. Wang, X.; Xu, Q.; Huang, M.; Zhang, L.; Peng, Z. Effects of journal rotation and surface waviness on the dynamic performance of aerostatic journal bearings. *Tribol. Int.* **2017**, *112*, 1–9. [CrossRef]
25. Cai, J.L.; Hang, Y.F.; Xiang, G.; Wang, J.X.; Wang, L.W. Effects of wear and shaft-shape error defects on the tribo-dynamic response of water-lubricated bearings under propeller disturbance. *Phys. Fluids* **2022**, *34*, 077118. [CrossRef]
26. Pasichnyi, O.O.; Lavrinenko, V.I. The Influence of Circumferential Waviness of the Diamond Wheel Working Surface on the Machined Surface Roughness. *J. Superhard Mater.* **2019**, *41*, 278–280. [CrossRef]
27. Nikolakopoulos, P.; Papadopoulos, C. A study of friction in worn misaligned journal bearings under severe hydrodynamic lubrication. *Tribol. Int.* **2008**, *41*, 461–472. [CrossRef]
28. Tang, D.X.; Xiang, G.; Guo, J.; Cai, J.L.; Yang, T.Y.; Wang, J.X.; Han, Y.F. On the optimal design of staved water-lubricated bearings driven by tribo-dynamic mechanism. *Phys. Fluids* **2023**, *35*, 093611. [CrossRef]
29. Guo, J.; Ding, B.; Wang, Y.F.; Han, Y.F. Co-optimization for hydrodynamic lubrication and leakage of V-shape textured bearings via linear weighting summation. *Phys. Scr.* **2023**, *98*, 125218. [CrossRef]
30. Sun, F.; Zhang, X.; Wang, Z.; Sun, Z.; Wang, D. Effects of shaft shape errors on the dynamic characteristics of a rotor-bearing system. *J. Tribol.* **2019**, *141*, 101701. [CrossRef]
31. Chen, S.A.; Xiang, G.; Fillon, M.; Guo, J.; Wang, J.X.; Cai, J.L. On the tribo-dynamic behaviors during start-up of water lubricated bearing considering imperfect journal. *Tribol. Int.* **2022**, *174*, 107685. [CrossRef]
32. Khonsari, M.M.; Booser, E.R. Proper film thickness key to bearing survival. *Mach. Des.* **2006**, *78*, 100–105.
33. Yang, T.Y.; Xiang, G.; Cai, J.L.; Wang, L.W.; Lin, X.; Wang, J.X.; Zhou, G.W. Five-DOF nonlinear tribo-dynamic analysis for coupled bearings during start-up. *Int. J. Mech. Sci.* **2024**, *269*, 109068. [CrossRef]
34. Song, Y.K.; Xiao, K.; Xiang, G. Entropy-based fluid–solid–thermal coupled wear prediction of journal bearing during repeated starting and stopping. *Wear* **2024**, *536–537*, 205157. [CrossRef]
35. Kogut, L.; Etsion, I. A finite element based elastic-plastic model for the contact of rough surfaces. *Tribol. Trans.* **2003**, *46*, 383–390. [CrossRef]
36. Tang, D.X.; Xiao, K.; Xiang, G.; Cai, J.L.; Fillon, M.; Wang, D.F.; Su, Z.L. On the nonlinear time-varying mixed lubrication for coupled spiral microgroove water-lubricated bearings with mass conservation cavitation. *Tribol. Int.* **2024**, *193*, 109381. [CrossRef]
37. Beheshti, A.; Khonsari, M. An Engineering Approach for the Prediction of Wear in Mixed Lubricated Contacts. *Wear* **2013**, *308*, 121–131. [CrossRef]
38. Han, Y.F.; Chan, C.; Wang, Z. Effects of Shaft Axial Motion and Misalignment on the Lubrication Performance of Journal Bearings Via a Fast Mixed EHL Computing Technology. *Tribol. Trans.* **2015**, *58*, 247–259. [CrossRef]
39. Wang, Q.; Shi, F.H.; Lee, S.C. A Mixed-TEHD Model for Journal-Bearing Conformal Contact—Part II: Contact, Film Thickness, and Performance Analyses. *J. Tribol.* **1998**, *120*, 206–213. [CrossRef]
40. Vincent, B.; Maspeyrot, P.; Frene, J. Cavitation in Noncircular Journal Bearings. *Wear* **1997**, *207*, 122–127. [CrossRef]

41. Kucinschi, B.R.; Fillon, M.; Frˆene, J.; Pascovici, M.D. A Transient Thermoelastohydrodynamic Study of Steadily Loaded Plain Journal Bearings Using Finite Element Method Analysis. *J. Tribol.* **2000**, *122*, 219–226. [CrossRef]
42. Cha, M.; Kuznetsov, E.; Glavatskih, S. A comparative linear and nonlinear dynamic analysis of compliant cylindrical journal bearings. *Mech. Mach. Theory* **2013**, *64*, 80–92. [CrossRef]